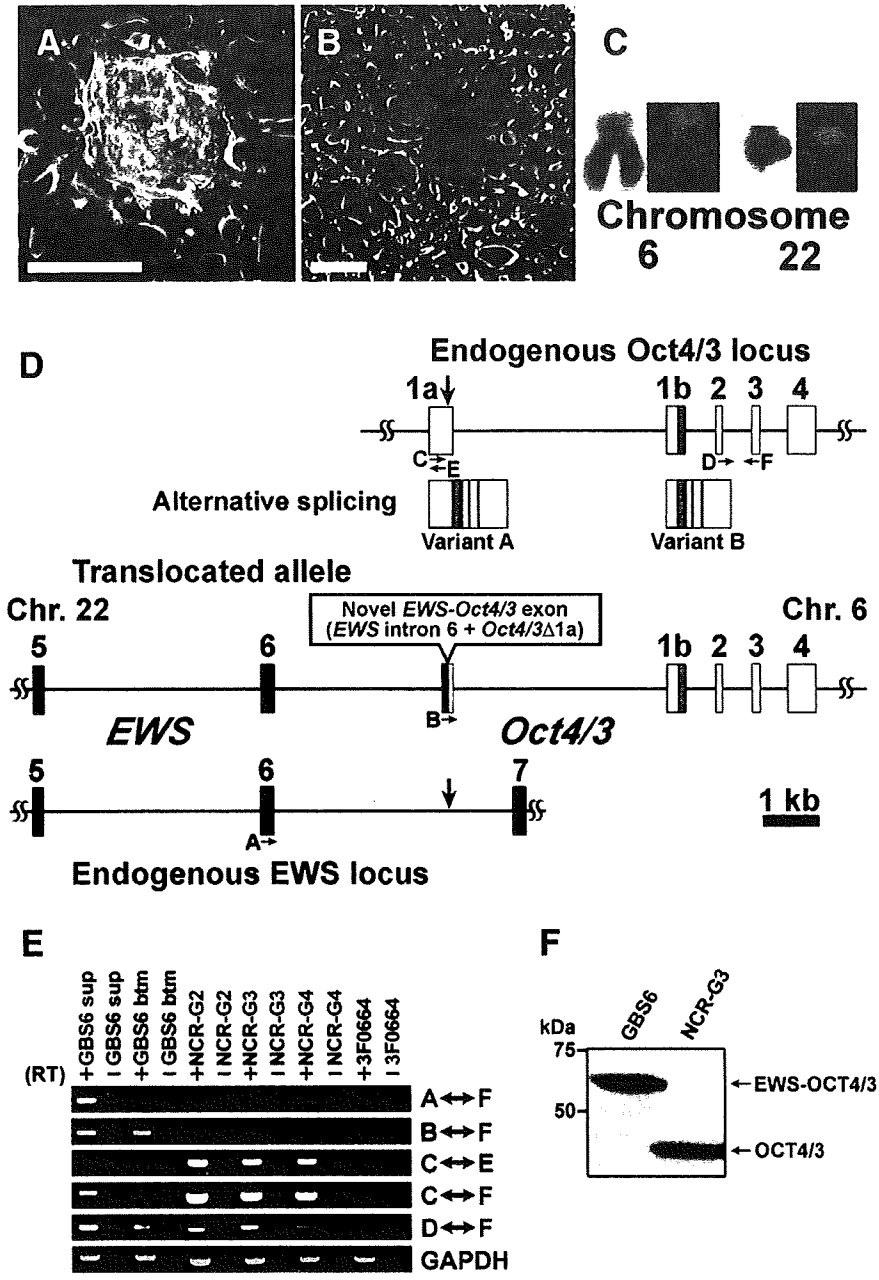

Fig. 1 – Phase contrast micrograph of GBS6 cells, and expression of the translocated *POU5F1/OCT4/3* gene. A cell line termed "GBS6" was generated from primary or first passage cells of a pelvic tumor [31]. (A) GBS6 cell aggregate (GBS6 sup). Scale bar: 100 μm. (B) GBS6 adherent cells (GBS6 btm). Scale bar: 100 μm. (C) G-banding karyotypic analysis and Spectral karyotyping (SKY) analysis of the translocated chromosomes. (D) Schematic representation of the *EWS-OCT4/3* structure in the t(6;22) tumor. *EWS* exons are represented by black boxes and *OCT4/3* exons by open boxes. The *OCT4/3*-1b exon is composed of an open and gray box. The novel *EWS-OCT4/3* chimeric exon is created by the fusion between *EWS* intron 6 and part of the exon of *OCT4/3* (Δ1a). The vertical arrows indicate each breakpoint on either chromosome 22 (*EWS*) or chromosome 6 (*OCT4/3*). The horizontal arrows indicate the position and direction of primers for PCR (Table 1). (E) RT-PCR analysis of the translocated *OCT4/3* gene and the untranslocated *OCT4/3* gene in GBS6 cell, NCR-G2, NCR-G3, NCR-G4, and 3F0664 cells. NCR-G2, NCR-G3, and NCR-G4 cells are embryonal carcinoma cells, and 3F0664 cells are mesenchymal cells. (F) Western blot analysis of EWS-OCT4/3 in GBS6 cells. Western blot analysis was performed using anti-Oct4/3 antibody. EWS-OCT4/3 chimeric protein (~58 kDa) was detected in GBS6 cells. The positions of prestained molecular markers (BIO-RAD) are indicated to the left (kDa).

HLA-ABC (IM1838, Beckman), HLA-DR, DP, DQ (6604366, Beckman), SSEA-1 (MAB4301, Chemicon), SSEA-3 (MAB4303, Chemicon), SSEA-4 (MAB4304, Chemicon), STRO-1 (MAB1038, R and D Systems), TRA-1-60 (MAB4360, Chemicon), and TRA-1-81 (MAB4381, Chemicon) were adopted as primary antibodies. PE-conjugated anti-mouse Ig antibody (550589, Pharmingen), PE-conjugated anti-mouse IgM antibody (555584, Pharmingen) and PE-conjugated anti-rat Ig antibody (550767, Pharmingen) were used as secondary antibodies. X-Mean, the sum of the intensity divided by total cell number, was automatically calculated, and it was adopted for the evaluation of this experiment.

Implantation of cells into mice

GBS6 cells ($>1\times10^7$) were subcutaneously inoculated into an immunodeficient, NOD/Shi-*scid*, IL-2Rγ^{null} mouse (NOG mouse) (CREA, Tokyo, Japan). Subcutaneous specimens were resected at 2 weeks after implantation. The operation protocols were accepted by the Laboratory Animal Care and the Use Committee of the National Research Institute for Child and Health Development, Tokyo (approval number: 2003-002 and 2005-003).

Immunohistochemistry analysis

Immunohistochemical analysis was performed as previously described [34–36] with antibodies to MIC2 (clone# 12E7, cat# M3601, DAKO, Carpinteria, CA, USA), vimentin (clone# V9, cat# M0725, DAKO, Carpinteria, CA, USA), neurofilament protein 70 kDa (NF-L, clone# 2F11, cat# M0762, DAKO, Carpinteria, CA, USA), desmin (clone# D9, cat# 010031, Bio-Science Products AG, Emmenbruecke, Switzerland), smooth muscle actin (clone# 1A4, cat# M0851, DAKO, Carpinteria, CA, USA), and OCT4/3 (clone# C-10, cat# sc-5279, Santa Cruz Biotechnology, Inc., CA, USA) in PBS containing 1% bovine serum albumin. As a methodological control, the primary antibody was omitted. Immunohistochemical analysis of iPS cells was performed according to the manufacturer's protocol [SCR002,

A

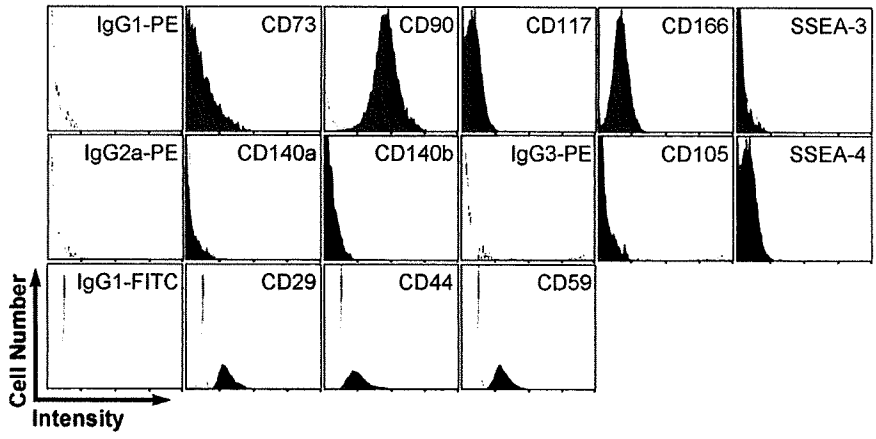

B

Negative (y≦0.1)			Low (0.1<y<1)	Positive (1<y)
CD13	CD106	ABCG2	CD73	CD9
CD14	CD117	HLA-DR,DQ,DP	CD166	CD29
CD24	CD130	SSEA-1		CD44
CD31	CD133	SSEA-3		CD59
CD34	CD135	SSEA-4		CD81
CD45	CD140a	Stro-1		CD90
CD50	CD140b	TRA-1-60		HLA-A,B,C
CD55	CD157	TRA-1-81		
CD105	CD243			

Fig. 2 – Cell surface marker analysis of GBS6 cells. (A) Flow cytometric analysis of cell surface markers in GBS6 cells. The results of CD73, CD90, CD117, CD166 and SSEA-3 were compared with the result of their isotype control, PE-conjugated IgG1. The results of CD140a and CD140b were compared with the result of PE-conjugated IgG2a. The results of CD105 and SSEA-4 were compared with the result of PE-conjugated IgG3. The results of CD29, CD44 and CD59 were compared with the result of FITC-conjugated IgG1. *X*-axis and *Y*-axis indicate the intensity and the cell number, respectively. (B) Summary of cell surface markers. "*y*" is "X-means" subtracted by 'a value of isotype control'; "$y<0.1$", "$0.1<y<1$", and "$1<y$" were determined "negative", "low" and "positive", respectively.

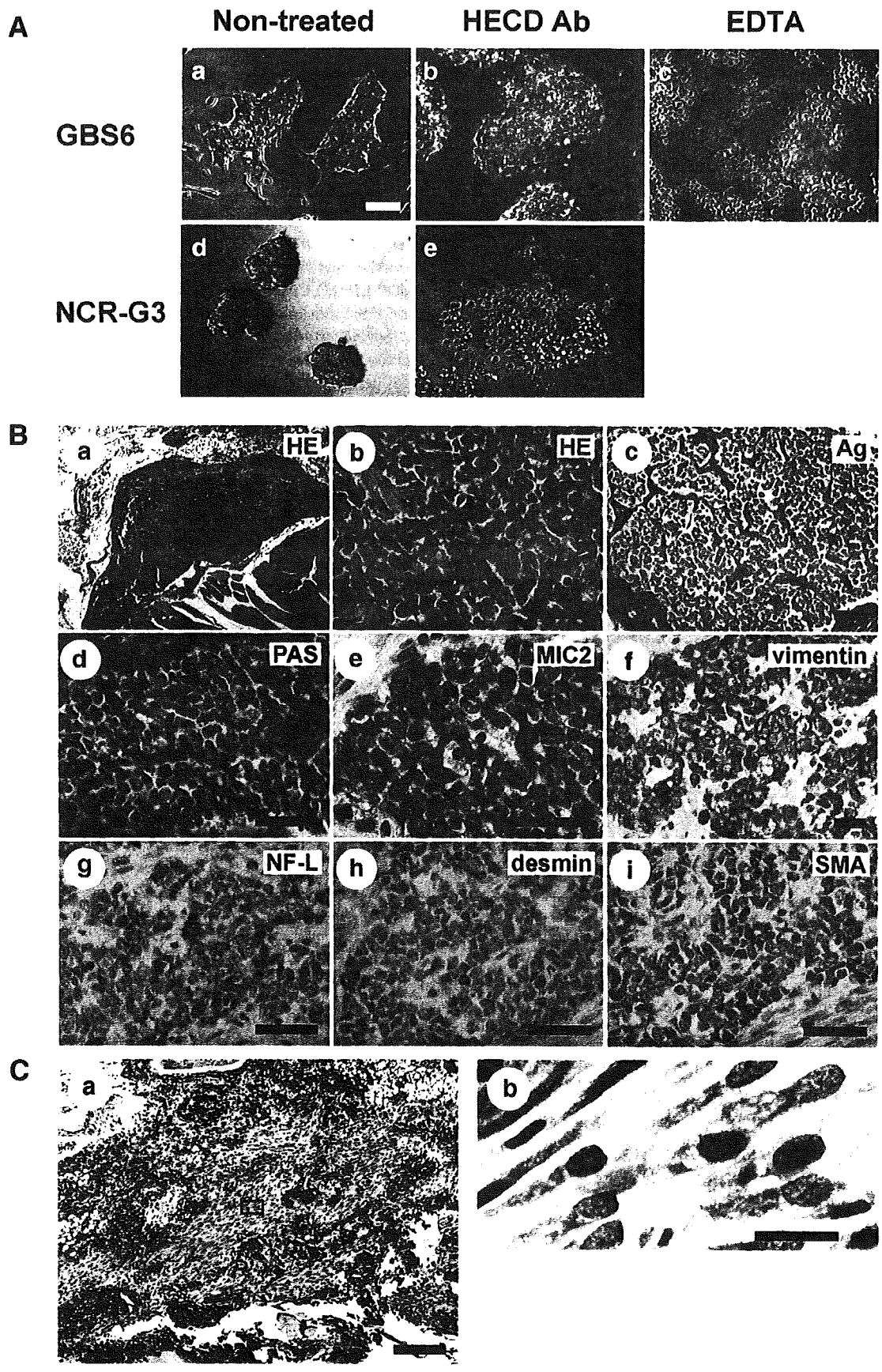
A
Non-treated
HECD Ab
EDTA
GBS6
NCR-G3
a
b
c
d
e
B
HE
HE
Ag
PAS
MIC2
vimentin
NF-L
desmin
SMA
C
a
b

Chemicon (Millipore)]. Primary antibodies included Oct-3/4 (C-10) (diluted at 1:300, sc-5279, Santa Cruz), NANOG (diluted at 1:300, RCAB0003P, ReproCELL), SSEA-4 (diluted at 1:300, MAB4304, CHEMICON), and TRA-1-60 (diluted at 1:300, MAB4360, CHEMICON). Secondary antibodies used were Alexa Fluor 546 Goat Anti-mouse IgG, 2 mg/mL (diluted at 1:300, A11003, Invitrogen), Alexa Fluor 488 Goat Anti-rabbit IgG, 2 mg/mL (diluted at 1:300, A11008, Invitrogen), and Alexa Fluor 488 Goat Anti-mouse IgG, 2 mg/mL, F (ab')2 fragment (diluted at 1:300, A11017, Invitrogen). Nuclei were stained with 1 μg/mL DAPI (40043, Biotium).

Quantitative RT-PCR

RNA was extracted from cells using the RNeasy Plus Mini kit (Qiagen). An aliquot of total RNA was reverse transcribed by using an oligo (dT) primer. For the thermal cycle reactions, the cDNA template was amplified (ABI PRISM 7900HT Sequence Detection System) using the Platinum Quantitative PCR SuperMix-UDG with ROX (11743-100, Invitrogen) under the following reaction conditions: 40 cycles of PCR (95 °C for 15 s and 60 °C for 1 min) after an initial denaturation (95 °C for 2 min). Fluorescence was monitored during every PCR cycle at the annealing step. The authenticity and size of the PCR products were confirmed using a melting curve analysis (using software provided by Applied Biosystems) and a gel analysis. mRNA levels were normalized using *GAPDH* as a housekeeping gene. POU5F1-2-F and POU5F1-3-R primers were used to detect the *OCT4/3* gene (see Table 1, D and F).

Chromatin immunoprecipitation (ChIP) assays

Chromatin immunoprecipitation was performed according to the instructions of the EZ ChIP Chromatin Immunoprecipitation Kit (17-371, Upstate Biotechnology Inc., Chicago, IL, USA). Histone and DNA were cross-linked with 1% formaldehyde for 10 min at room temperature and formaldehyde was then inactivated by the addition of 125 mM glycine. The chromatin was then sonicated to an average DNA fragment length of 200 to 1000 bp. Soluble chromatin reacted with and without anti-acetylated Histone H3 (06-599, Upstate Biotechnology Inc., Chicago, IL, USA), and anti-acetylated Histone H4 (06-866, Upstate Biotechnology Inc., Chicago, IL, USA). The immunocomplex was purified and collected in elution buffer (0.1 M $NaHCO_3$, 1% sodium dodecyl sulfate). Crosslinking was then reversed using elution buffer containing RNase A (0.03 mg/mL) and NaCl (0.3 M) by incubation for 4 h at 65 °C. Supernatant obtained without antibody was used as the input control. The DNA was treated with proteinase K for 1 h at 45 °C and purified. For all ChIP experiments, quantitative PCR analyses were performed in real time as described in this manuscript. Relative occupancy values were calculated by determining the apparent immunoprecipitation efficiency (ratios of the amount of immunoprecipitated DNA to that of the input sample) and normalized to the level observed at a control region. For all the primers used, each gave a single product of the right size adult stem cell confirmed by agarose gel electrophoresis and dissociation curve analysis. These primers also gave no DNA product in the no-template control. The following three primer sets for human *OCT4/3*, as previously described [26], were adopted for real-time PCR to quantitate the ChIP-enriched DNA: human *POU5F1*-A (-2613/-2396), 5′-GGG GAACCTGGAGGATGG-CAAGCTGAGAAA-3′ and 5′-GGCCTGGTGGGGGTGGGAGG AACAT-3′; human *POU5F1*-B (-1779/-1563), 5-CCTGCACCCCTCCACAAATCACTC GC-3′ and 5′-TGCAATCCCCTCAAAGACTGAGCCTCAGAC-3′ ; human *POU5F1*-C (-237/-136), 5′-GAGGGGCGCCAGTTGTGTCTCCCGGTTTT-3′ and 5′-GGGAGGTGGG GGGAGAAACTGAGGCGAAGG-3′.

DNA methylation analysis

The NCR-G2 (JCRB cell bank number; JCRB1167) [32], NCR-G3 (JCRB cell bank number; JCRB1168) [32], GBS6, and Yub636BM (human bone marrow cells derived from an extra digit) cells were prepared for this assay. Genomic DNA was isolated using DNeasy Blood and Tissue Kit (69504, QIAGEN). Primers were selected from the CpG island regions with homogenous CpG site methylation patterns. The target region of the genes used for methylation analysis and the primer sequences used for PCR amplification are shown in Table 4. One of the two primers in the PCR amplification of the target regions is tagged with a T7 promoter sequence: cagtaatacgactcactatagggagaaggct. The PCR reactions were carried out in a total volume of 5 μL using 1 pmol of each primer, 40 μM dNTP, 0.1 U HotStar Taq DNA polymerase (QIAGEN), 1.5 mM $MgCl_2$, 5× PCR buffer (final concentration 1×), and bisulfite-converted DNA. The reaction mix was preactivated for 15 min at 95 °C. The reactions were amplified in 45 cycles of 95 °C for 20 s, 62 °C for 30 s, and 72 °C for 30 s followed by 72 °C for 3 min. Unincorporated dNTPs were dephosphorylated by adding 1.7 μL DNase-free water and 0.3 U Shrimp Alkaline Phosphatase (SAP). The reaction was incubated at 37 °C for 20 min and SAP was then heat-inactivated for 10 min at 85 °C. Typically, 2 μL of the PCR reaction was directly used as a template in a 6.5 μL combined transcription-cleavage reaction. Twenty units of T7 polymerase (Epicentre) were used to incorporate either dCTP or dTTP in the transcripts. Ribonucleotides at 1 mM and the dNTP substrate at 2.5 mM were used. RNase A (Sequenom) was included to cleave the in vitro transcript. The mixture was then further diluted with water to a final volume of 27 μL. Conditioning of the phosphate backbone prior to MALDI-TOF MS was achieved by the addition of 6 mg CLEAN resin (Sequenom). The cleavage reaction samples (15 nL) were dispensed onto silicon

Fig. 3 – In vitro and in vivo characteristics of GBS6 cells. (A) Ca++-dependent, E-cadherin-independent adhesion of GBS6 cell aggregates. GBS6 cells (a) were unaffected by the antibody to E-cadherin (b), but were dissociated by EDTA, Ca++ chelator (c). In contrast, NCR-G3 cells (d), serving as a control since they are E-cadherin-dependent, were dissociated and induced to death by the antibody to E-cadherin (e). Scale bar: 100 μm. (B) Immunohistochemical analysis of GBS6 cells implanted into the subcutaneous tissue of NOG mice. GBS6 cells at 2 weeks after implantation (a, b: hematoxylin and eosin stain, c: silver stain, d: PAS stain) were examined for immunohistochemical analysis using antibodies to MIC2 (e), vimentin (f), neurofilament protein 70 kDa (g: NF-L), desmin (h), and smooth muscle actin (i: SMA). Scale bars: 200 μm (a) and 50 μm (b–i). (C) Immunohistochemical analysis with the anti-OCT4/3 antibody of GBS6 cells implanted into the subcutaneous tissue of NOG mice. GBS6 cells at 2 weeks after implantation were examined for immunohistochemical analysis using antibodies to OCT4/3. The higher-magnification image of the region enclosed by a square in "a" (b). Scale bars: 200 μm (a) and 20 μm (b).

chips preloaded with matrix (SpectroCHIP, Sequenom). Mass spectra were collected using a MassARRAY mass spectrometer (Sequenom). Spectra were analyzed using proprietary peak picking and spectra interpretation tools (EpiTYPER, Sequenom).

For analysis of DNA methylation, we examined the methylation-dependent C/T sequence changes introduced by bisulfite treatment. Those C/T changes are reflected as G/A changes on the reverse strand and hence result in a mass difference of 16 kDa for

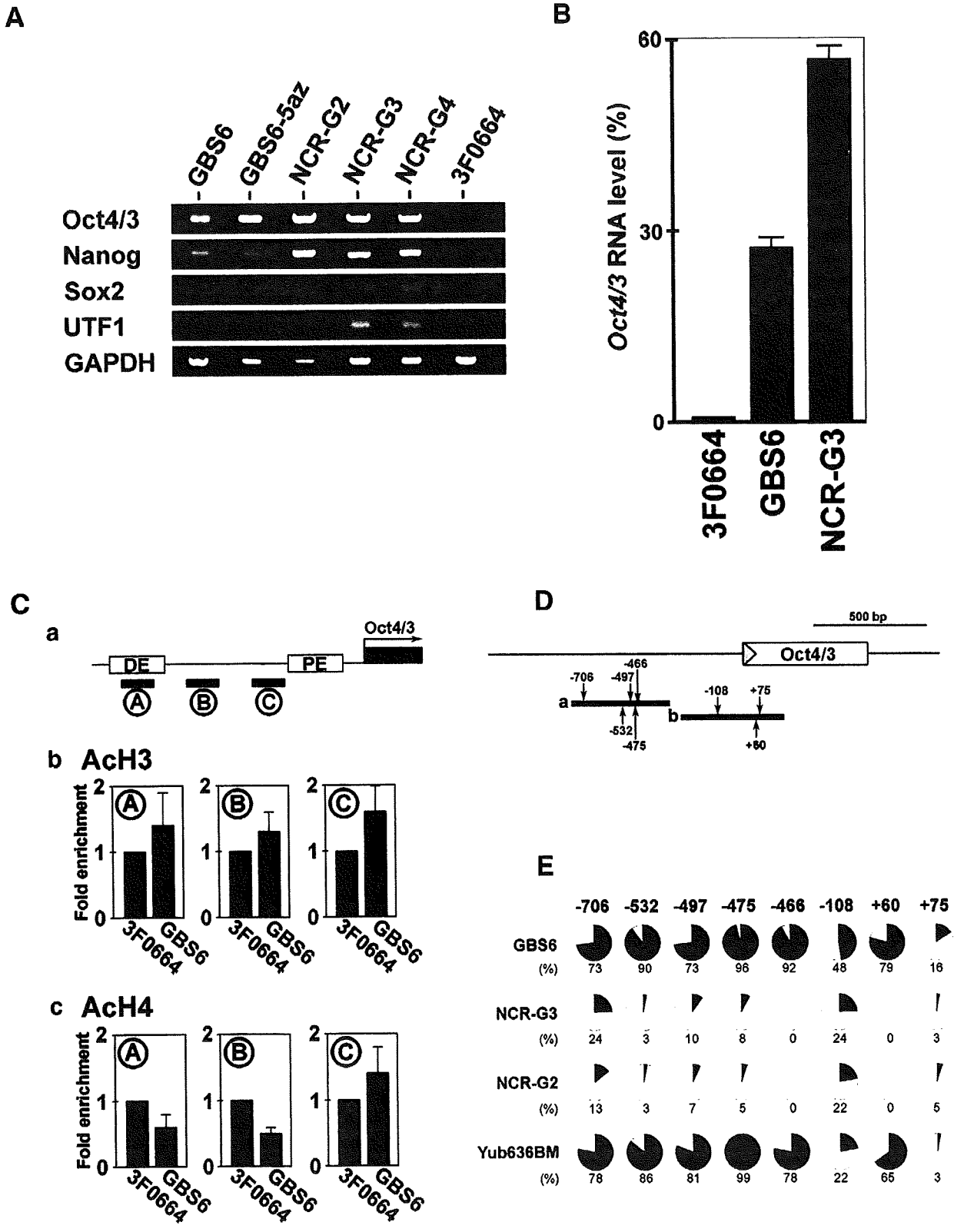

each CpG site enclosed in the cleavage products generated from the RNA transcript. The mass signals representing nonmethylated DNA and those representing methylated DNA, built signal pairs, which are representative for the CpG sites within the analyzed sequence substring. The intensities of the peaks were compared, and the relative amount of methylated DNA was calculated from this ratio. The method yields quantitative results for each of these sequence-defined analytic units referred to as CpG units, which contain either one individual CpG site or an aggregate of subsequent CpG sites.

Plasmid construction

Each open reading frame of human *OCT4/3* and *SOX2* was amplified by RT-PCR using the RNA extracted from NCR-G2 cells (JCRB cell bank number; JCRB1167) [32], a complex-type germ cell tumor cell line. Also, those of *c-MYC* and *KLF4* were amplified by RT-PCR using the RNA extracted from the bone marrow stromal cell line, UET13. A Gateway cassette composed of an attR1/R2 flanked CmR and ccdB (Invitrogen) was amplified by PCR and ligated into the Eco RI/Not I site of pMXs retroviral expression vector to create pMXs-DEST [37]. PCR amplification was performed by using KOD-Plus-DNA polymerase (KOD-201, TOYOBO). The constructs were confirmed by sequencing.

Retroviral infection and iPS cell generation

293FT cells (Invitrogen) were plated at 2×10^6 cells per 100 mm dish and incubated overnight. The next day, the cells were co-transfected with pMXs-OCT4/3, pMXs-SOX2, pMXs-c-MYC, pMXs-KLF4, pCL-GagPol, and pHCMV-VSV-G vectors with TransIT-293 reagent (Mirus, Madison, WI). Twenty-four hours after transfection, the medium was replaced with a new medium, which was collected after 48 h as the virus-containing supernatant. MRC-5 cells were seeded at 1×10^5 cells per 35 mm dish 1 day before infection. The virus-containing supernatants were filtered through a 0.45 μm pore-size filter, ultracentrifuged at 8500 rpm for 16 h, and then resuspended in DMEM (D6429, SIGMA) supplemented with 4 mg/mL polybrene (Nacalai Tesque). Equal amounts of concentrated supernatants containing each of the four retroviruses were mixed, transferred to MRC-5 cells, and incubated for 8 h. The MRC-5 cells were cultured for 4 days and replated on an irradiated MEF feeder layer in 100 mm dish. The medium was replaced with the iPSellon medium supplemented with 10 ng/mL bFGF. One-half of the medium was changed every day and the cells were cultured up to 30 days after a day of infection. Colonies were picked up and transferred into 0.2 mL of iPSellon medium when colonies appeared. The colonies were mechanically dissociated to small clumps by pipeting up and down or mechanically cut using a STEMPRO EZPassage disposable passaging tool (23181010, Invitrogen). The cell suspension was transferred on irradiated MEF feeder in 4-well plates [176740, Nunc (Thermo Fisher Scientific)]. We define this stage as passage 1.

Teratoma formation

iPS cells were harvested by accutase treatment, collected into tubes, and centrifuged, and the pellets were suspended in the iPSellon medium. The same volume of Basement Membrane Matrix (354234, BD Biosciences) was added to the cell suspension. Cells (1×10^7) were implanted subcutaneously to a BALB/c-*nu*/*nu* mouse (CREA, Japan) for 4 weeks. Tumors were dissected and fixed with PBS containing 4% paraformaldehyde. Paraffin-embedded tissue was sliced and stained with hematoxylin and eosin.

GeneChip expression analysis

Total RNA was extracted from cells using the RNeasy Mini Kit (74104, Qiagen, Valencia, CA). Genomic DNA was eliminated by DNase I (2215A, TAKARA BIO INC.) treatments. From all RNA samples, 5 μg of total RNA was used as a starting material for the microarray sample preparation. Double-stranded cDNA was synthesized from DNase-treated total RNA, and the cDNA was subjected to in vitro transcription in the presence of biotinylated nucleoside triphosphates using the Enzo BioArray HighYield RNA Transcript Labeling Kit (Enzo Life Sciences, Inc., Farmingdale, NY), according to the manufacturer's protocol (One-Cycle Target Labeling and Control Reagent package). Human-genome-wide gene expression was examined with the Human Genome U133A Probe array (GeneChip, Affymetrix), which contains the oligonucleotide probe set for approximately 23,000 full-length genes and expressed sequence tags (ESTs), according to the manufacturer's protocol (Expression Analysis Technical Manual and GeneChip small sample target labeling Assay Version 2 technical note, http://www.affymetrix.com/support/technical/index.affx) as previously described [5]. Hierarchical clustering and principle component

Fig. 4 – Expression of the *OCT4/3* gene and histone modification of the *OCT4/3* promoter in GBS6 cells. (A) Expression of embryonic stem cell-enriched genes in GBS6, NCR-G2, NCR-G3, NCR-G4, and 3F0664 cells. GBS6 cells expressed the *OCT4/3* and *NANOG* genes, but not the *SOX2* and *UTF1* genes. NCR-G2 cells expressed the *OCT4/3* and *NANOG* genes; both NCR-G3 cells and NCR-G4 cells expressed the *OCT4/3*, *NANOG*, *SOX2* and *UTF1* genes. 3F0664 mesenchymal cells did not express these four kinds of embryonic stem cell-enriched genes. POU5F1-1a-F and POU5F1-1a-R (Table 1) were used to amplify the endogenous *OCT4/3* gene. (B) Quantitative PCR analysis to assess the expression level of *OCT4/3* mRNA in GBS6. *OCT4/3* mRNA level is expressed relative to 3F0664 cells control. (C) Real-time PCR to quantitate the ChIP-enriched DNA using acetylated Histone H3 and acetylated Histone H4 antibodies. Schematic of the location of the amplicons (A–C) used to detect ChIP-enriched fragments in *OCT4/3* shown relative to the distal enhancer (DE)/CR4 region, to the proximal enhancer (PE), and to transcription start site (arrow) (a). The relative levels of acetylated Histone H3 (b) and acetylated Histone H4 (c) modifications were detected in GBS6 cells and 3F0664 cell control. GBS6 cells are represented by black bars and 3F0664 cells by open bars. (D) DNA methylation analysis in the promoter region of the *OCT4/3* gene. The target regions of *OCT4/3* used for the quantitative DNA methylation analysis. Region 'a' and Region 'b' include 5 (−706, −532, −497, −475, −466) and 3 (−108, +60, +75) CpG sites, respectively. The positions of CpG sites are relative to the *OCT4/3* transcription start site (gray triangle). (E) The relative amount of methylated DNA ratio (%) at each CpG site is indicated as the black area in the pie chart.

analysis were performed to group mesenchymal cells obtained from bone marrow into subcategories (http://lgsun.grc.nia.nih.gov/ANOVA/).

Results

Establishment of human cells of mesenchymal origin with overexpression of the translocated POU5F1/OCT4/3 gene

To investigate whether cells of mesenchymal origin acquire an embryonic phenotype, a novel human cell line termed GBS6 was established from the pelvic bone tumor, of which histology shows diffuse proliferation of undifferentiated tumor cells with oval nuclei and scant but short spindle cytoplasm [31]. The generated cells grew attached to the dish as a polygonal cell sheet with cell aggregates forming in the center (Figs. 1A, B), and retained the reciprocal translocation, t(6; 22), detected in the original tumor (Fig. 1C). The *EWS-OCT4/3* chimeric gene expression also remained (Figs. 1D, E and Table 1). Embryonal carcinoma (EC) cells, i.e., NCR-G2, NCR-G3, and NCR-G4, served as control cells expressing the endogenous *OCT4/3* gene. Immunoblot analysis revealed that EWS-OCT4/3 fusion protein was expressed in GBS6 cells (Fig. 1F).

Cell surface markers of GBS6 cells

GBS6 cell surface markers were evaluated by flow cytometric analysis (Fig. 2). The results showed that GBS6 cells were strongly positive (Positive; Fig. 2B) for CD9, CD29 (integrin β1), CD44, CD59, CD81, CD90 (Thy-1) and HLA-A,B,C (HLA class I); weakly positive (Low; Fig. 2B) for CD73 and CD166 (ALCAM); negative (Negative; Fig. 2B) for CD55, CD105 (endogrin), CD140a (PDGFRα), and CD140b (PDGFRβ). The lack of CD13, CD55, CD105, CD106, CD140a, and CD140b in GBS6 cells suggests that the surface markers of GBS6 cells are different from those of conventional mesenchymal cells [10,38,39].

E-cadherin-independent growth of GBS6 cells

To investigate whether GBS6 cells survive dependent on E-cadherin-like human embryonic cells, the cells were treated by an inhibitory antibody to E-cadherin (HECD Ab) and EDTA (Fig. 3A). GBS6 cell survival was unaffected by the E-cadherin antibody but affected by EDTA (Fig. 3A-a, b, c). In contrast, NCR-G3 cells, human embryonal carcinoma cells that proliferate in an E-cadherin-dependent manner, were dissociated and induced to apoptosis by the E-cadherin antibody (Fig. 3A-d, e).

Implantation of GBS6 cells into immunodeficient mice

To investigate an in vivo phenotype of GBS6 cells, the cells were intramuscularly injected into immunodeficient NOG mice and examined by histopathology and immunohistochemistry (Fig. 3B). The injected cells exhibited an undifferentiated phenotype with oval nuclei and scant spindle cytoplasm (Fig. 3B-b), and showed an alveolar configuration (Fig. 3B-c). The cells were negative by the PAS stain (Fig. 3B-d). The cells were immunohistochemically positive for MIC2 and vimentin (Fig. 3B-e, f), and negative for neurofilament, desmin, and smooth muscle actin (Fig. 3B-g, h, i). The cells retained OCT4/3 in their nuclei even after implantation (Fig. 3C).

Expression of ES-enriched genes

To determine if GBS6 cells express ES cell-enriched genes, that is, the *OCT4/3*, *NANOG*, *SOX2*, and *UTF1* genes, RT-PCR with specific primer sets (Table 2) and gene chip analyses were performed. GBS6 cells expressed the endogenous *OCT4/3* and *NANOG* genes like NCR-G2, NCR-G3, and NCR-G4 embryonal carcinoma cells, but did not express the *SOX2* and *UTF1* genes (Fig. 4A). The results of the RT-PCR analysis were compatible with those of the gene chip analysis (GSE8113, Table 3). To compare the expression level of stem cell-specific genes in GBS6 cells, ES cells, and mesenchymal cells, we performed a quantitative RT-PCR analysis. The expression level of *OCT4/3* was about half that of human EC cells, but was more than twenty-five times that of 3F0664 mesenchymal cells (Fig. 4B). The results show that the expression level of *OCT4/3* is comparable to that of human EC cell.

To determine if the cis-regulatory element of the *OCT4/3* gene has so-called open chromatin structure, we performed the chip analysis using antibodies to acetylated H3 and acetylated H4 (Fig. 4C). The results show that acetylated histone levels which the *OCT4/3* promoter is wrapped around in GBS6 cells are comparable with those in 3F0664 mesenchymal cells. We also performed methylation analysis of the *OCT4/3* gene in GBS6 cells because the expression of *OCT4/3* gene is regulated by methylation (Figs. 4D, E and Table 4). The promoter region of the *OCT4/3* gene was heavily methylated in GBS6 cells as compared with human NCR-G3 embryonal carcinoma cells expressing the *OCT4/3* gene at a high level.

Cell reprogramming assay

To investigate if chimeric EWS-OCT4/3 induces iPS cells like native OCT4/3, we performed Yamanaka's reprogramming assay on MRC-5 human fetal lung fibroblasts (Fig. 5A), using the chimeric *EWS-OCT4/3* construct with the *KLF-4*, *SOX2*, and *c-MYC* genes according to the conventional protocol [40] with some modifications. We failed to obtain iPS cells using the *EWS-OCT4/3*, *KLF-4*, *SOX2*, and *c-MYC* constructs (Fig. 5B), albeit trials of three independent experiments, whereas, for a control, we successfully generated 101 clones of iPS cells from MRC-5 cells using the *OCT4/3*, *KLF-4*, *SOX2*, and *c-MYC* constructs (Fig. 5C). The iPS cells generated from MRC-5 cells expressed human ES cell-specific surface antigens (Figs. 5D–G). In vivo implantation analysis showed that iPS cells generated various tissues including neural tissues (Fig. 5H: ectoderm), cartilage (Fig. 5I: mesoderm),

Table 4 – Primers used for PCR amplification of the bisulfite-converted DNA.

Name	Sequence	Size (bp)
Region 'a'	Forward: 5′ TTG GTT ATT GTG TTT ATG GTT GTT G 3′	437
	Reverse: 5′ TAA ACC AAA ACA ATC CTT CTA CTC C 3′	
Region 'b'	Forward: 5′ TTT GGG TAA TAA AGT GAG ATT TTG TTT 3′	452
	Reverse: 5′ CTA ACC CTC CAA AAA AAC CTT AAA A 3′	

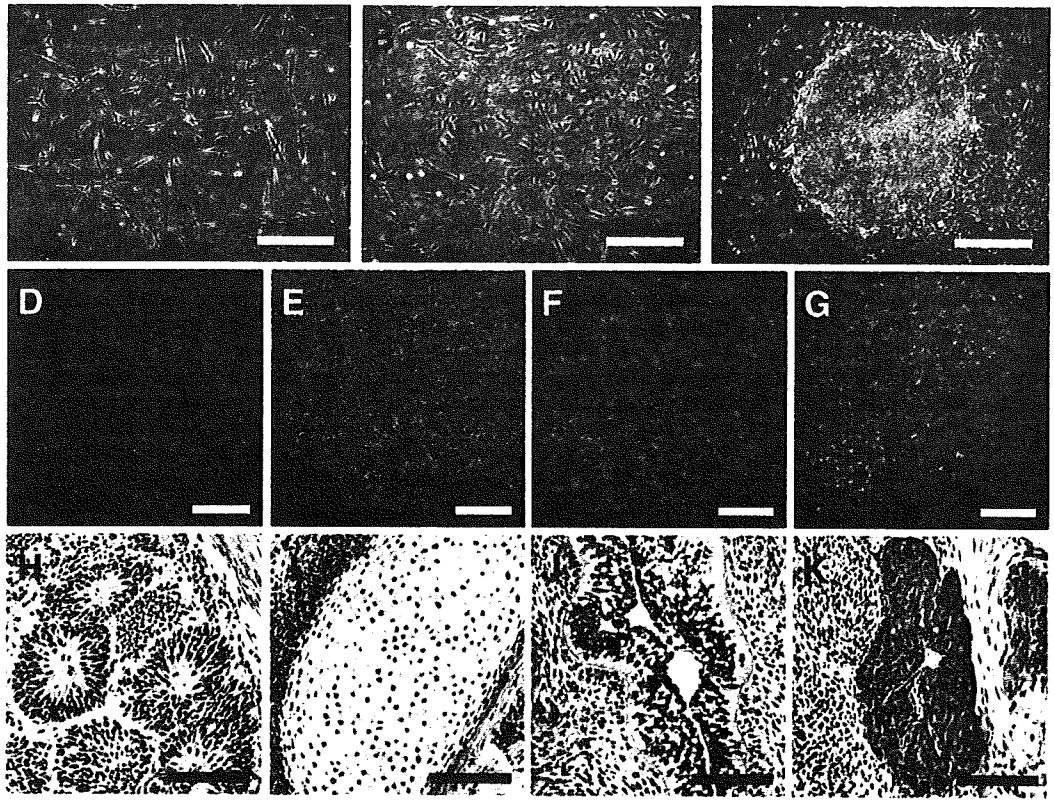

Fig. 5 – Induction of iPS cells from MRC-5 cells and teratoma formation. (A) Morphology of MRC-5 cells. (B) Morphology of cells using *EWS-OCT4/3*, *KLF-4*, *SOX2*, and *c-MYC* genes at Day 30 after infection. (C) Morphology of established iPS cell (clone 16: Fetch) colony using *OCT4/3*, *KLF-4*, *SOX2*, and *c-MYC* genes at Day 20 after infection. (D–G) Immunocytochemistry for OCT4/3 (D), NANOG (E), SSEA-4 (F), and TRA-1-60 (G). Nuclei were stained with DAPI. Bars = 500 μm (A–C), and 200 μm (D–G). In addition, chromosomal G-band analyses showed that human iPS cells from MRC-5 had a normal karyotype of 46XY (not shown). The analysis of short tandem repeat shows that novel iPS cells from MRC-5 cells were not a result of cross-contamination. Hematoxylin and eosin staining of teratoma derived from the generated iPS cells. Cells (1×10^7) were implanted subcutaneously to a BALB/c-*nu/nu* mouse for 4 weeks. Histological examination showed that the tumor contained various tissues, neural tissues (H; ectoderm), cartilage (I; mesoderm), a gut-like epithelial tissue (J; endoderm), and a hepatic tissue (K; endoderm). Bars = 100 μm (H–K).

a gut-like epithelial tissue (Fig. 5J: endoderm), and a hepatic tissue (Fig. 5K: endoderm). These results imply that the chimeric *EWS-OCT4/3* gene does not participate in reprogramming of somatic cells.

Principle component analysis of global gene expression in GBS6 cells

To determine whether GBS6 cells are categorized into embryonal cells or mesenchymal cells, global gene expression patterns of GBS6 cells, embryonal carcinoma cells (NCR-G2, NCR-G3, and NCR-G4), yolk sac tumor cells (NCR-G1), and marrow stromal cells (3F0664, H4-1, and Yub10F) were further analyzed by principle component analysis (PCA), which reduces high-dimensionality data into a limited number of principle components (Fig. 6). The first principle component (PC1) captures the largest contributing factor of variation, which characterizes the differential expression of genes. As we were interested in the differential gene expression component, we plotted the position of each cell type against the PC1, PC2, and PC3 axis in three-dimensional space by using virtual reality modeling language (Fig. 6A). Close examination of the 3D model identified PC1 as the most representative view of the 3D model. PC1 axis direction is therefore used to characterize the differential gene expression (Fig. 6B). In addition, hierarchical analysis of the cells analyzed for global gene expression revealed that GBS6 cells are categorized into embryonal carcinoma cells and yolk sac tumor cells, i.e., NCR-G1, -G2, -G3, and -G4 cells (Fig. 6C).

Discussion

In this study, we generated a cell line with a transitional form between mesenchymal cells and embryonic stem cells. Loss of mesenchyme-specific cell markers, i.e., CD13, CD55, CD105, CD106, CD140a and CD140b, and modification of cell survival with the calcium chelator indicate that GBS6 cells are no longer mesenchymal cells. Global and drastic differences in gene expression with the GeneChip analysis support the conclusion that GBS6 cells no longer exhibit the profile of mesenchymal cells. It is also noteworthy that this transition phenotype is reliably inherited ex vivo after a series of in vitro passages.

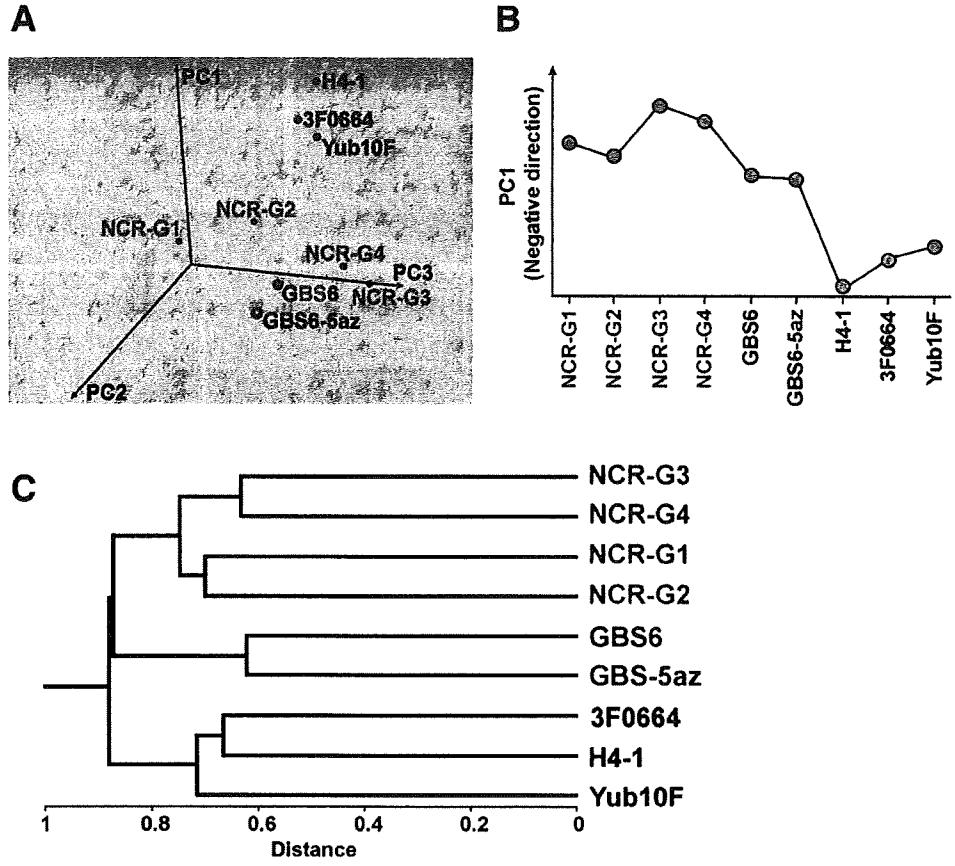

Fig. 6 – Principal component analysis and hierarchical clustering of gene expression in GBS6 cells, embryonal carcinoma cells, and bone marrow cells. (A) 3D-representation of principle component analysis. (B) Principal components of PC1 axis, negative direction. (C) Hierarchical clustering analysis of averages.

OCT4/3 function and its physiological partner EWS in embryonic transition

ES-like cells or iPS cells are generated from murine fibroblasts by transfecting four genes, i.e., *OCT4/3*, *SOX2*, *KLF-4* and *c-MYC* are necessary for the mesenchymal–embryonic transition [1–3]. However, OCT4/3 alone is not sufficient to confer embryonic phenotypes to human bone marrow-derived cells, NIH3T3 cells (data not shown) or embryonic fibroblasts [1]. EWS and OCT4/3 are directly bound both in vitro and in vivo [41]; in other words, EWS is a binding partner of OCT4/3. Therefore, the EWS-OCT4/3 protein in GBS6 cells is considered a fusion between physiological partners. EWS and OCT4/3 are co-expressed in the pluripotent mouse and human ES cells. To investigate if the EWS-OCT4/3 has a transcriptional activity, we performed the luciferase assay. The results show that the chimeric *EWS-OCT4/3* gene has comparable or higher transcriptional activity than the native *OCT4/3* gene does (Supplementary Fig. S1). Ectopic expression of non-chimeric EWS enhances the transactivation activity of OCT4/3; the N-terminal QSY domain of EWS and the C-terminal POU domain function as a transcriptional activation and DNA binding, respectively [42,43]. The *OCT4/3* gene is overexpressed under the cis-regulatory element of the *EWS* gene [31], and the functional co-operation of OCT4/3 and EWS at a protein level to transcriptional activation may lead to embryonic transformation in GBS6 cells. Converting mesenchymal cells to embryonic cells opposes the usual direction of ES cell differentiation [44]; and this is achieved by chimeric OCT4/3 with physiological co-activator EWS driven by the potent cis-regulatory element of the *EWS* gene [31]. This phenotypic conversion requires the molecular reprogramming of mesenchymal cells with new instructions.

Mesenchymal to embryonic "incomplete" transition by overexpression of chimeric OCT4/3

OCT4/3 fused to *EWS* not only participates in oncogenesis [29,31], but also contributes to mesenchymal–embryonic transition, at least in part from the viewpoint of global gene expression profiles and cell surface markers (Figs. 2 and 6). GBS6 cells are subcategorized into groups of cells derived from testicular germ cell tumors (Fig. 6A, cells with embryonic phenotypes are shown in pink), and the PC1 axis indicates transition from mesenchymal cell group to embryonal cell group (Fig. 6B). This transition was, however, incomplete; some of the ES-specific genes were not reactivated. OCT4/3 is a member of the POU family of transcription factors, is expressed in pluripotent ES cells, including primordial germ cells [17–21], and functions as a master switch in differentiation by regulating cells that have, or can develop, pluripotent

potential. However, tight chromatin structure in GBS6 cells may render OCT4/3 recognition sequences inaccessible [45]. The OCT4/3 recognition sequences have been found in the cis-regulatory elements of the FGF-4 and CD140a/platelet-derived growth factor receptor-α gene [46], but GBS6 cells are indeed negative for CD140a (Fig. 2B). Alternatively, the lack of other essential transcription factors such as SOX2 and UTF1 (Fig. 4A, Table 3) and/or co-factors may be a cause of "incomplete" transition. Interestingly, this transition phenotype is reliably inherited ex vivo after a series of in vitro passages, and this may also be attributed to the function of OCT4/3 that is critical for self-renewal of embryonic stem cells [24].

Mesenchymal to epithelial transition is observed in physiological and pathological conditions [47–50]. In contrast, mesenchymal–embryonic transition has been achieved in an artificial experimental condition in vitro [1–3]. Homogenous positive staining for OCT4/3 in embryonal carcinoma cells supports the model that the encoded protein is crucial, and the absence of OCT4/3 in non-embryonal carcinoma cells is in agreement with the inability to generate pluripotent stem cells [51]. The cell line generated in this study with overexpression of chimeric OCT4/3, although this is just one case of rare human immortalized cells, provides us with insight into cell plasticity involving OCT4/3 that is essential for ES cell maintenance and into the complexity required for changing cellular identity.

Acknowledgments

We would like to express our sincere thanks to Michiyo Nasu for histological analysis, Yoriko Takahashi for data mining, and Kayoko Saito for secretary work. This study was supported by grants from the Ministry of Education, Culture, Sports, Science and Technology (MEXT) of Japan and Health and Labor Sciences Research Grants; by Research on Health Science Focusing on Drug Innovation from the Japan Health Science Foundation; by the Program for Promotion of Fundamental Studies in Health Science of the Pharmaceuticals and Medical Devices Agency; by the grant from Terumo Life Science Foundation; by a research Grant for Cardiovascular Disease from the Ministry of Health, Labor and Welfare; and by a Grant for Child Health and Development from the Ministry of Health, Labor and Welfare.

Appendix A. Supplementary data

Supplementary data associated with this article can be found, in the online version, at doi:10.1016/j.yexcr.2009.06.016.

REFERENCES

[1] K. Takahashi, S. Yamanaka, Induction of pluripotent stem cells from mouse embryonic and adult fibroblast cultures by defined factors, Cell 126 (2006) 663–676.
[2] K. Okita, T. Ichisaka, S. Yamanaka, Generation of germline-competent induced pluripotent stem cells, Nature 448 (2007) 313–317.
[3] M. Wernig, A. Meissner, R. Foreman, T. Brambrink, M. Ku, K. Hochedlinger, B.E. Bernstein, R. Jaenisch, In vitro reprogramming of fibroblasts into a pluripotent ES-cell-like state, Nature 448 (2007) 318–324.
[4] M.J. Go, C. Takenaka, H. Ohgushi, Forced expression of Sox2 or Nanog in human bone marrow derived mesenchymal stem cells maintains their expansion and differentiation capabilities, Exp. Cell Res. 314 (2008) 1147–1154.
[5] T. Mori, T. Kiyono, H. Imabayashi, Y. Takeda, K. Tsuchiya, S. Miyoshi, H. Makino, K. Matsumoto, H. Saito, S. Ogawa, M. Sakamoto, J. Hata, A. Umezawa, Combination of hTERT and bmi-1, E6, or E7 induces prolongation of the life span of bone marrow stromal cells from an elderly donor without affecting their neurogenic potential, Mol. Cell. Biol. 25 (2005) 5183–5195.
[6] R.H. Lee, B. Kim, I. Choi, H. Kim, H.S. Choi, K. Suh, Y.C. Bae, J.S. Jung, Characterization and expression analysis of mesenchymal stem cells from human bone marrow and adipose tissue, Cell. Physiol. Biochem. 14 (2004) 311–324.
[7] J.G. Toma, M. Akhavan, K.J. Fernandes, F. Barnabe-Heider, A. Sadikot, D.R. Kaplan, F.D. Miller, Isolation of multipotent adult stem cells from the dermis of mammalian skin, Nat. Cell Biol. 3 (2001) 778–784.
[8] C.H. Cui, T. Uyama, K. Miyado, M. Terai, S. Kyo, T. Kiyono, A. Umezawa, Menstrual blood-derived cells confer human dystrophin expression in the murine model of duchenne muscular dystrophy via cell fusion and myogenic transdifferentiation, Mol. Biol. Cell 18 (2007) 1586–1594.
[9] O.K. Lee, T.K. Kuo, W.M. Chen, K.D. Lee, S.L. Hsieh, T.H. Chen, Isolation of multipotent mesenchymal stem cells from umbilical cord blood, Blood 103 (2004) 1669–1675.
[10] M. Terai, T. Uyama, T. Sugiki, X.K. Li, A. Umezawa, T. Kiyono, Immortalization of human fetal cells: the life span of umbilical cord blood-derived cells can be prolonged without manipulating p16INK4a/RB braking pathway, Mol. Biol. Cell 16 (2005) 1491–1499.
[11] X. Zhang, A. Mitsuru, K. Igura, K. Takahashi, S. Ichinose, S. Yamaguchi, T.A. Takahashi, Mesenchymal progenitor cells derived from chorionic villi of human placenta for cartilage tissue engineering, Biochem. Biophys. Res. Commun. 340 (2006) 944–952.
[12] E.H. Allan, P.W. Ho, A. Umezawa, J. Hata, F. Makishima, M.T. Gillespie, T.J. Martin, Differentiation potential of a mouse bone marrow stromal cell line, J. Cell. Biochem. 90 (2003) 158–169.
[13] H. Imabayashi, T. Mori, S. Gojo, T. Kiyono, T. Sugiyama, R. Irie, T. Isogai, J. Hata, Y. Toyama, A. Umezawa, Redifferentiation of dedifferentiated chondrocytes and chondrogenesis of human bone marrow stromal cells via chondrosphere formation with expression profiling by large-scale cDNA analysis, Exp. Cell Res. 288 (2003) 35–50.
[14] S. Makino, K. Fukuda, S. Miyoshi, F. Konishi, H. Kodama, J. Pan, M. Sano, T. Takahashi, S. Hori, H. Abe, J. Hata, A. Umezawa, S. Ogawa, Cardiomyocytes can be generated from marrow stromal cells in vitro, J. Clin. Invest. 103 (1999) 697–705.
[15] N. Nishiyama, S. Miyoshi, N.M. Hida, T. Uyama, K. Okamoto, Y. Ikegami, K. Miyado, K. Segawa, M. Terai, M. Sakamoto, S. Ogawa, A. Umezawa, The significant cardiomyogenic potential of human umbilical cord blood-derived mesenchymal stem cells in vitro, Stem Cells 25 (2007) 2017–2024.
[16] J. Deng, B.E. Petersen, D.A. Steindler, M.L. Jorgensen, E.D. Laywell, Mesenchymal stem cells spontaneously express neural proteins in culture and are neurogenic after transplantation, Stem Cells 24 (2006) 1054–1064.
[17] H.R. Scholer, G.R. Dressler, R. Balling, H. Rohdewohld, P. Gruss, Oct-4: a germline-specific transcription factor mapping to the mouse t-complex, EMBO J. 9 (1990) 2185–2195.
[18] K. Okamoto, H. Okazawa, A. Okuda, M. Sakai, M. Muramatsu, H. Hamada, A novel octamer binding transcription factor is differentially expressed in mouse embryonic cells, Cell 60 (1990) 461–472.
[19] M.H. Rosner, M.A. Vigano, K. Ozato, P.M. Timmons, F. Poirier, P.W. Rigby, L.M. Staudt, A POU-domain transcription factor in early

stem cells and germ cells of the mammalian embryo, Nature 345 (1990) 686–692.
[20] M.F. Pera, D. Herszfeld, Differentiation of human pluripotent teratocarcinoma stem cells induced by bone morphogenetic protein-2, Reprod. Fertil. Dev. 10 (1998) 551–555.
[21] T. Goto, J. Adjaye, C.H. Rodeck, M. Monk, Identification of genes expressed in human primordial germ cells at the time of entry of the female germ line into meiosis, Mol. Hum. Reprod. 5 (1999) 851–860.
[22] M. Pesce, X. Wang, D.J. Wolgemuth, H. Scholer, Differential expression of the Oct-4 transcription factor during mouse germ cell differentiation, Mech. Dev. 71 (1998) 89–98.
[23] J. Nichols, B. Zevnik, K. Anastassiadis, H. Niwa, D. Klewe-Nebenius, I. Chambers, H. Scholer, A. Smith, Formation of pluripotent stem cells in the mammalian embryo depends on the POU transcription factor Oct4, Cell 95 (1998) 379–391.
[24] H. Niwa, J. Miyazaki, A.G. Smith, Quantitative expression of Oct-3/4 defines differentiation, dedifferentiation or self-renewal of ES cells, Nat. Genet. 24 (2000) 372–376.
[25] B. Abdel-Rahman, M. Fiddler, D. Rappolee, E. Pergament, Expression of transcription regulating genes in human preimplantation embryos, Hum. Reprod. 10 (1995) 2787–2792.
[26] J.L. Chew, Y.H. Loh, W. Zhang, X. Chen, W.L. Tam, L.S. Yeap, P. Li, Y.S. Ang, B. Lim, P. Robson, H.H. Ng, Reciprocal transcriptional regulation of Pou5f1 and Sox2 via the Oct4/Sox2 complex in embryonic stem cells, Mol. Cell. Biol. 25 (2005) 6031–6046.
[27] O. Delattre, J. Zucman, B. Plougastel, C. Desmaze, T. Melot, M. Peter, H. Kovar, I. Joubert, P. de Jong, G. Rouleau, A. Aurias, G. Thomas, Gene fusion with an ETS DNA-binding domain caused by chromosome translocation in human tumours, Nature 359 (1992) 162–165.
[28] F. Urano, A. Umezawa, W. Hong, H. Kikuchi, J. Hata, A novel chimera gene between EWS and E1A-F, encoding the adenovirus E1A enhancer-binding protein, in extraosseous Ewing's sarcoma, Biochem. Biophys. Res. Commun. 219 (1996) 608–612.
[29] F. Mitelman, B. Johansson, F. Mertens, The impact of translocations and gene fusions on cancer causation, Nat. Rev. Cancer 7 (2007) 233–245.
[30] M. Kuroda, T. Ishida, M. Takanashi, M. Satoh, R. Machinami, T. Watanabe, Oncogenic transformation and inhibition of adipocytic conversion of preadipocytes by TLS/FUS-CHOP type II chimeric protein, Am. J. Pathol. 151 (1997) 735–744.
[31] S. Yamaguchi, Y. Yamazaki, Y. Ishikawa, N. Kawaguchi, H. Mukai, T. Nakamura, EWSR1 is fused to POU5F1 in a bone tumor with translocation t(6;22)(p21;q12), Genes Chromosomes Cancer 43 (2005) 217–222.
[32] J. Hata, J. Fujimoto, E. Ishii, A. Umezawa, Y. Kokai, Y. Matsubayashi, H. Abe, S. Kusakari, H. Kikuchi, T. Yamada, T. Maruyama, Differentiation of human germ cell tumor cells in vivo and in vitro. Acta Histochem. Cytochem. 25 (1992) 563–576.
[33] E. Schrock, T. Veldman, H. Padilla-Nash, Y. Ning, J. Spurbeck, S. Jalal, L.G. Shaffer, P. Papenhausen, C. Kozma, M.C. Phelan, E. Kjeldsen, S.A. Schonberg, P. O'Brien, L. Biesecker, S. du Manoir, T. Ried, Spectral karyotyping refines cytogenetic diagnostics of constitutional chromosomal abnormalities, Hum. Genet. 101 (1997) 255–262.
[34] M. Sano, A. Umezawa, H. Abe, A. Akatsuka, S. Nonaka, H. Shimizu, M. Fukuma, J. Hata, EAT/mcl-1 expression in the human embryonal carcinoma cells undergoing differentiation or apoptosis, Exp. Cell Res. 266 (2001) 114–125.
[35] S. Gojo, N. Gojo, Y. Takeda, T. Mori, H. Abe, S. Kyo, J. Hata, A. Umezawa, In vivo cardiovasculogenesis by direct injection of isolated adult mesenchymal stem cells, Exp. Cell Res. 288 (2003) 51–59.
[36] T. Sugimoto, A. Umezawa, J. Hata, Neurogenic potential of Ewing's sarcoma cells, Virchows Arch. 430 (1997) 41–46.
[37] Y. Miyagawa, H. Okita, H. Nakaijima, Y. Horiuchi, B. Sato, T. Taguchi, M. Toyoda, Y.U. Katagiri, J. Fujimoto, J. Hata, A. Umezawa, N. Kiyokawa, Inducible expression of chimeric EWS/ETS proteins confers Ewing's family tumor-like phenotypes to human mesenchymal progenitor cells, Mol. Cell. Biol. 28 (2008) 2125–2137.
[38] B.L. Yen, H.I. Huang, C.C. Chien, H.Y. Jui, B.S. Ko, M. Yao, C.T. Shun, M.L. Yen, M.C. Lee, Y.C. Chen, Isolation of multipotent cells from human term placenta, Stem Cells 23 (2005) 3–9.
[39] E.K. Waller, J. Olweus, F. Lund-Johansen, S. Huang, M. Nguyen, G.R. Guo, L. Terstappen, The "common stem cell" hypothesis reevaluated: human fetal bone marrow contains separate populations of hematopoietic and stromal progenitors, Blood 85 (1995) 2422–2435.
[40] K. Takahashi, K. Tanabe, M. Ohnuki, M. Narita, T. Ichisaka, K. Tomoda, S. Yamanaka, Induction of pluripotent stem cells from adult human fibroblasts by defined factors, Cell 131 (2007) 861–872.
[41] J. Lee, B.K. Rhee, G.Y. Bae, Y.M. Han, J. Kim, Stimulation of Oct-4 activity by Ewing's sarcoma protein, Stem Cells 23 (2005) 738–751.
[42] D. Zhang, A.J. Paley, G. Childs, The transcriptional repressor ZFM1 interacts with and modulates the ability of EWS to activate transcription, J. Biol. Chem. 273 (1998) 18086–18091.
[43] S.L. Palmieri, W. Peter, H. Hess, H.R. Scholer, Oct-4 transcription factor is differentially expressed in the mouse embryo during establishment of the first two extraembryonic cell lineages involved in implantation, Dev. Biol. 166 (1994) 259–267.
[44] T. Barberi, L.M. Willis, N.D. Socci, L. Studer, Derivation of multipotent mesenchymal precursors from human embryonic stem cells, PLoS Med. 2 (2005) e161.
[45] H. Kimura, M. Tada, N. Nakatsuji, T. Tada, Histone code modifications on pluripotential nuclei of reprogrammed somatic cells, Mol. Cell. Biol. 24 (2004) 5710–5720.
[46] H.J. Kraft, S. Mosselman, H.A. Smits, P. Hohenstein, E. Piek, Q. Chen, K. Artzt, E.J. van Zoelen, Oct-4 regulates alternative platelet-derived growth factor alpha receptor gene promoter in human embryonal carcinoma cells, J. Biol. Chem. 271 (1996) 12873–12878.
[47] R. Kalluri, E.G. Neilson, Epithelial–mesenchymal transition and its implications for fibrosis, J. Clin. Invest. 112 (2003) 1776–1784.
[48] C. Martinez-Alvarez, M.J. Blanco, R. Perez, M.A. Rabadan, M. Aparicio, E. Resel, T. Martinez, M.A. Nieto, Snail family members and cell survival in physiological and pathological cleft palates, Dev. Biol. 265 (2004) 207–218.
[49] H. Peinado, F. Portillo, A. Cano, Transcriptional regulation of cadherins during development and carcinogenesis, Int. J. Dev. Biol. 48 (2004) 365–375.
[50] E. de Laplanche, K. Gouget, G. Cleris, F. Dragounoff, J. Demont, A. Morales, L. Bezin, C. Godinot, G. Perriere, D. Mouchiroud, H. Simonnet, Physiological oxygenation status is required for fully differentiated phenotype in kidney cortex proximal tubules, Am. J. Physiol. Renal Physiol. 291 (2006) F750–760.
[51] L.H. Looijenga, H. Stoop, H.P. de Leeuw, C.A. de Gouveia Brazao, A.J. Gillis, K.E. van Roozendaal, E.J. van Zoelen, R.F. Weber, K.P. Wolffenbuttel, H. van Dekken, F. Honecker, C. Bokemeyer, E.J. Perlman, D.T. Schneider, J. Kononen, G. Sauter, J.W. Oosterhuis, POU5F1 (OCT3/4) identifies cells with pluripotent potential in human germ cell tumors, Cancer Res. 63 (2003) 2244–2250.

The Journal of Immunology

IL-10 Is a Negative Regulatory Factor of CAWS-Vasculitis in CBA/J Mice as Assessed by Comparison with Bruton's Tyrosine Kinase-Deficient CBA/N Mice

Noriko N. Miura, Motohiko Komai, Yoshiyuki Adachi, Naoki Osada, Yosuke Kameoka, Kazuo Suzuki and Naohito Ohno

J. Immunol. 2009;183;3417-3424; originally published online Aug 12, 2009;
doi:10.4049/jimmunol.0802484
http://www.jimmunol.org/cgi/content/full/183/5/3417

The Journal of Immunology is published twice each month by The American Association of Immunologists, Inc., 9650 Rockville Pike, Bethesda, MD 20814-3994.

Print ISSN: 0022-1767 Online ISSN: 1550-6606.

IL-10 Is a Negative Regulatory Factor of CAWS-Vasculitis in CBA/J Mice as Assessed by Comparison with Bruton's Tyrosine Kinase-Deficient CBA/N Mice[1]

Noriko N. Miura,* Motohiko Komai,* Yoshiyuki Adachi,* Naoki Osada,† Yosuke Kameoka,† Kazuo Suzuki,§‡ and Naohito Ohno[2]*

***Candida albicans* water-soluble fraction (CAWS), a mannoprotein-β-glucan complex obtained from the culture supernatant of *C. albicans* NBRC1385, exhibits vasculitis-inducing activity (CAWS-vasculitis) in mice. The sensitivity to CAWS-vasculitis varies greatly among mouse strains. This study examined the factors contributing to or inhibiting CAWS-vasculitis using CAWS-vasculitis-resistant CBA/J mice and Bruton's tyrosine kinase-deficient CBA/N mice, which is a CAWS-vasculitis-sensitive strain that has the same origin as CBA/J mice. After stimulation with various kinds of pathogen-associated molecular patterns, the production of inflammatory cytokines IL-6 and IFN-γ was induced in CBA/N mice, whereas that of immunosuppressive IL-10 was induced in CAWS-vasculitis-resistant CBA/J mice. Furthermore, the production of tissue inhibitor of metalloproteinase 1, an endogenous matrix metalloproteinase inhibitor, was observed in CBA/J mice. The results strongly suggest that the difference in the production of these cytokines is closely linked to the development of CAWS-vasculitis. *The Journal of Immunology*, 2009, 183: 3417–3424.**

Vasculitis syndrome is a collective term for diseases caused by vasculitis, which is defined as inflammation of the vascular wall (endothelium, tunica media, and adventitia) and its adjacent parts. In arteries and veins, vasculitis is characterized by the localized infiltration of inflammatory cells into the intravascular wall and its surroundings, accompanied by denaturation and necrosis. Many diseases, including Takayasu's disease, Wegener's granulomatosis, and Buerger's disease, are known to cause vasculitis. However, the cause of various clinical pathologies or groups of disorders brought about by vasculitis remains unknown. The techniques of molecular biology and genetic engineering are well established, and new technologies have been developed frequently in these fields. Using such technologies, the etiology and pathology of vasculitis is being clarified gradually.

Kawasaki disease was first reported by Dr. T. Kawasaki in 1967 and is also called acute febrile mucocutaneous lymph node syndrome (1). It is a disease characterized by fever continuing for 5 days or longer, hyperemia of bulbar conjunctiva in both eyes, strawberry tongue, and atypical rash; the cause of which is unknown. Systemic vasculitis develops in Kawasaki disease patients. In particular, vasculitis of the coronary artery as sequela is of concern (2). The coronary vasculitis develops further into coronary aneurysm. If the aneurysm is relatively small, it can be normalized within 1 or 2 years in most cases. However, a large aneurysm may result in occlusion by forming a thrombus, complicated with myocardial ischemia and myocardial disorders, and lead to sudden death because of myocardial infarction. In regard to this occasionally lethal vasculitis, although the incidence of coronary disorders has been on the decline because of recently introduced gammaglobulin therapy, neither the pathogenic mechanism nor therapeutic pharmacological mechanism is known (3, 4).

Murata and colleagues et al. (5–7) revealed that arteritis similar to coronary vasculitis, which is known as a sequela of Kawasaki disease, can be induced in mice by *Candida albicans*-derived substances in the forms of a KOH extract of *C. albicans* cell wall. Subsequently, *C. albicans* water-soluble fraction (CAWS)[3] was studied for its ability to induce vasculitis, and it was found to induce vasculitis at a higher rate than *C. albicans*-derived substances. The results indicated that CAWS is very useful for the analysis of the pathogenesis of this disease (8–15).

A deficiency of Bruton's tyrosine kinase (Btk) in humans causes serious sequela. This condition is known as X-linked agammaglobulinemia. Patients with X-linked agammaglobulinemia are vulnerable to infection, and administration of Ig is indicated (16). In mouse, the lack of Btk is called Xid (*xid*), and CBA/N mice have this genetic background (17).

CBA/J and CBA/N mice were differentiated from CBA/H mice, which were derived from DBA mice. In CBA/N mice, several phenomena caused by the lack of Btk have been reported. Btk is believed to be essential for B cell differentiation and maturation. In

*Laboratory for Immunopharmacology of Microbial Products, Tokyo University of Pharmacy and Life Sciences, Tokyo, Japan; †Laboratory of Genetic Resources, National Institute of Biomedical Innovation, Osaka, Japan; ‡National Institute of Infectious Diseases, Tokyo, Japan; and §Graduate School of Medicine and School of Medicine, Chiba University, Chiba, Japan

Received for publication August 6, 2008. Accepted for publication July 4, 2009.

The costs of publication of this article were defrayed in part by the payment of page charges. This article must therefore be hereby marked *advertisement* in accordance with 18 U.S.C. Section 1734 solely to indicate this fact.

[1] This work was partly supported by a grant-in-aid for Scientific Research from the Ministry of Education, Culture, Sports, Science, and Technology of Japan and the Promotion and Mutual Aid Corporation for Private Schools (Japan). This study was also supported by the Ministry of Health, Labour, and Welfare of Japan by a Grant for "Research on Regulatory Science of Pharmaceuticals and Medical Devices" and by the Program for Promotion of Basic and Applied Researches for Innovations in Bio-oriented Industry.

[2] Address correspondence and reprint requests to Dr. Naohito Ohno, Laboratory for Immunopharmacology of Microbial Products, Tokyo University of Pharmacy and Life Sciences, 1432-1 Horinouchi, Hachioji, Tokyo 192-0392, Japan. E-mail address: ohnonao@ps.toyaku.ac.jp

[3] Abbreviations used in this paper: CAWS, *Candida albicans* water-soluble fraction; Btk, Bruton's tyrosine kinase; EVG, Elastica-van-Gieson; MMP, matrix metalloprotease; PAF, platelet-activating factor; PAMP, pathogen-associated molecular pattern; TIMP1, tissue inhibitor of metalloproteinase 1.

www.jimmunol.org/cgi/doi/10.4049/jimmunol.0802484

particular, this enzyme is reported to participate in rearrangement of the L chain gene during pre-B cell differentiation into immature B cells. Consequently, few mature B cells exist in CBA/N mice, and their Ab-producing ability is decreased (18–20). Other effects of the lack of Btk include a decrease in NO production in macrophages, an increase in IL-12 production, and a decrease in IL-5 production from T cells (21, 22).

This study examined the ability of CAWS to induce vasculitis in CBA/N mice, histologically analyzed CBA/N and CAWS-vasculitis-resistant CBA/J mice, and compared the difference in cytokine responses and the inflammatory parameters between CBA/N and CAWS-vasculitis-resistant CBA/J mice. CAWS-vasculitis inhibitory factors were also analyzed.

Materials and Methods

Experimental animals

Male CBA/N and DBA/2 mice were acquired from Japan SLC. Male CBA/J mice were acquired from Charles River Japan. The animals were raised in a specific pathogen-free environment. Mice aged 5–14 wk were used in this study. All animal experiments in Tokyo University of Pharmacy and Life Sciences (TUPLS), and each of the experimental protocols was approved by the Committee of Laboratory Animal Experiments of TUPLS.

Fungi

C. albicans strain NBRC1385 was acquired from the National Institute of Technology and Evaluation Biological Resource Center, stored on Sabouraud agar medium (Difco) at 25°C, and subcultured once every 3 mo.

Preparation of CAWS

CAWS was prepared from *C. albicans* strain NBRC1385 in accordance with conventional methods. Culture was performed in 5 liters of C-limiting medium for 2 days at a rotating speed of 400 rpm while pumping in air at 27°C and 5 L/min. After culturing, an equal volume of ethanol was added, and after allowing to stand undisturbed overnight, the precipitate was recovered. This fraction was dissolved in 250 ml of distilled water, ethanol was added, and the solubilized fraction was allowed to stand undisturbed overnight. The precipitate was recovered and dried with acetone to obtain CAWS.

Administration schedule for induction of CAWS-vasculitis

CAWS (0 or 4 mg/mouse) was administered i.p. for 5 consecutive days to each mouse. At 28 days after CAWS injection, mice were sacrificed, and the hearts of the animals were fixed with 10% neutral formalin and prepared in paraffin blocks. Tissue sections were stained with H&E stain or Elastica-van-Gieson (EVG) stain.

Examination of IL-10 and endogenous matrix metalloproteinase (MMP) inhibitor (tissue inhibitor of metalloproteinase 1 (TIMP1)) mRNA expression levels in aorta by RT-PCR

The spleen and the aorta were resected from mice, frozen in liquid nitrogen, and immediately stored in Isogen (Nippon Gene). Each sample was homogenized with a homogenizer, and RNA was isolated by chloroform extraction. The total RNA level was determined by measuring OD using Nanodrop-ND1000. All total RNA were stored at −80°C or below.

Nuclease-free water was added to the total RNA along with oligo dT_{20} primer (Promega), and the reaction was conducted in a Thermal Cycler (Takara) at 70°C for 5 min. The product was cooled immediately by placing the reaction on ice for 5 min. Then, the following reagents were added: Moloney murine leukemia virus reverse transcriptase XL (Promega), PCR nucleotide mix (dNTP) (Promega), Moloney murine leukemia virus reverse transcriptase 5× reaction buffer, and nuclease-free water. The reverse transcriptase reaction was performed at 42°C for 60 min in a total volume of 25 μl/tube to obtain cDNA. The obtained cDNA was used as a template by adding PCR Master Mix (2×) (Promega), forward primer, reverse primer, and nuclease-free water, and heat denaturation was performed at 94°C for 2 min. One cycle consisted of heat denaturation at 94°C for 10 s, primer annealing at 55°C for 30 s, and elongation at 72°C for 1 min. Thirty cycles of this reaction were performed to obtain the PCR products. The primer sequences are shown as follows, all of which were purchased from Sigma-Genosys: IL-10 forward primer, 5′-ACCTGGTAGAAGTGTATGCCCCAGGCA-3′; IL-10 reverse primer, 5′-CTATGCAGTTGATGAAGATGTCAAA-3′; TIMP1 forward primer, 5′-ACTCGGACCTGGTCATAAGGGC-3′; TIMP1 reverse primer, 5′-AAGAAGCTGCAGGCACTGAT-3′; β-actin forward primer, 5′-TGGAATCCTGTGGCATCCTGAAAC-3′; and β-actin reverse primer, 5′-TAAAACGCAGCTCAGTAACAGTCCG-3′.

Comprehensive analysis of expressed gene by gene chip

We pooled total RNA from the spleens of three DBA/2 and two CBA/J mice for each strain after 21 days from the injection of CAWS. The probes labeled by cyanin3 and cyanin5 were hybridized with a DNA microarray (mouse 10K oligo chip; DNA Chip Consortium) on which 10,386 clones were spotted. After washing, fluorescence was measured using an array scanner. The fluorescence intensity of each spot was corrected by subtracting the background fluorescence intensity. Genes of signal intensity values <1000 were excluded because these may be detected nonspecifically. The microarray data was deposited to Gene Expression Omnibus (accession no. GSE16529; (www.ncbi.nlm.nih.gov/geo/query/acc.cgi)).

Spleen cell culture

The mice were euthanized by inhalation of CO_2, after which the spleen was excised. After teasing using a mesh in RPMI 1640 medium, the tissue was separated by centrifugation at 1200 rpm by 5 min, and the resulting cells were treated with Ammonium Chloride Potassium lysing buffer (8.20 g/L NH_4Cl, 1 g/L $KHCO_3$, and 37.2 mg/L EDTA 2Na). After two washes with RPMI 1640 medium, the spleen cells were counted to adjust the cell density and then used after being suspended in RPMI 1640 medium with 10% FCS. The spleen cells were adjusted to 5×10^5 in RPMI 1640 medium containing 10% FCS, and 500-μl aliquots were added to each well of a 48-well plate. After the addition of LPS (from *Escherichia coli* serotype 0111:B4; SIGMA), CpG (1668; 5′-TCCATGACGTTCCTGATGCT-3′; Sigma-Genosys), or tri-acylated lipoproteine (Pam_3-CSK_4), the cells were cultured for 48 h in a 5% CO_2 incubator at 37°C. The cytokine level of the culture supernatant was determined by ELISA as described below.

Measurement of IL-10 and TIMP1

IL-10 level was measured using a OPT_{EIA} IL-10 ELISA kit (BD Pharmingen), and the TIMP1 level was measured using a RayBio Mouse TIMP1 ELISA kit.

Measurement of IFN-γ

A 96-well ELISA plate (Nunc) was coated with rat anti-mouse IFN-γ mAb (BD Pharmingen) using 0.1 M $NaHCO_3$ (pH 8.2) and incubated overnight at 4°C. After washing with 0.05% Tween PBS (PBST), the Ab was blocked for 40 min at 37°C with 0.5% BSA-PBST (BPBST). This was followed by the addition of standards and samples (50 μl each), incubation for 40 min at 37°C, and six washes with PBST. Fifty microliters of a secondary Ab in the form of biotinylated rat anti-mouse IFN-γ (1/1000; BD Pharmingen) was then added, and after incubation for 40 min at 37°C and a wash with PBST, peroxidase-conjugated streptavidin (1/2000; BD Pharmingen) was added. This was followed by incubation for 40 min at 37°C and six washes with PBST. Subsequently, color was generated using peroxidase substrate (tetramethylbenzidine microwell peroxidase substrate system; Kirkegaard & Perry Laboratories). After termination of the reaction with 1 M phosphoric acid, absorbance (OD450/reference OD630) was measured. Recombinant mouse IFN-γ (BD Pharmingen) was used as the standard.

Measurement of IL-6

A 96-well ELISA plate (Nunc) was coated with rat anti-mouse IL-6 mAb (BD Pharmingen) using 0.1 M bicarbonate buffer (pH 9.5) and incubated overnight at 4°C. After washing with PBST, the Ab was blocked for 40 min at 37°C with BPBST. This was followed by the addition of standards and samples (50 μl each), incubation for 40 min at 37°C, and six washes with PBST. Fifty microliters of a secondary Ab in the form of biotinylated rat anti-mouse IL-6 (1/2000; BD Pharmingen) was then added, and after incubation for 40 min at 37°C and a wash with PBST, peroxidase-conjugated streptavidin (1/10,000; BD Pharmingen) was added. This was followed by incubation for 40 min at 37°C and six washes with PBST. Subsequently, 50 μl of peroxidase substrate (tetramethylbenzidine microwell peroxidase substrate system; Kirkegaard & Perry Laboratories) was added to generated color, and absorbance was measured as described previously. Recombinant mouse IL-6 (BD Pharmingen) was used as the standard.

Test for significant difference

Tests for significant differences in this study were performed using Student's *t* test, and values with $p < 0.05$ were judged significant.

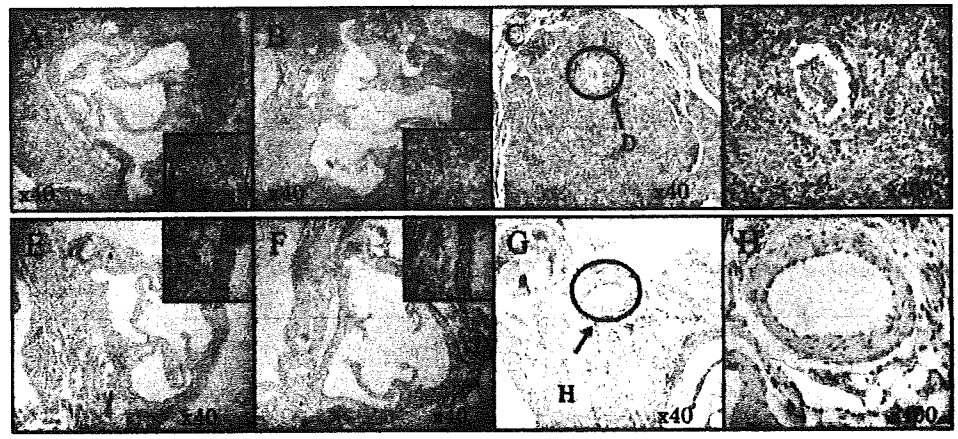

FIGURE 1. Histopathological findings of coronary arteries and aorta in CBA/N and CBA/J mice. CAWS (4 mg/mouse) was i.p. administered to CBA/N (*A–D*) and CBA/J (*E–H*) mice for 5 consecutive days. At 14 (*A* and *E*) and 28 (*B–D* and *F–H*) days after CAWS injections, mice were sacrificed and stained using H&E.

Results

Histological analysis of CAWS-vasculitis in CBA/J and CBA/N mice

Following the protocol for CAWS-vasculitis induction, CAWS was administered to CBA/J and CBA/N mice, and tissue slices of the beginning of aorta were prepared and stained with HE and EVG for observation. As a result, a 100% incidence of vasculitis was observed in the aorta and coronary artery of CBA/N mice (Fig. 1, *A–D*). This vasculitis in CBA/N mice developed 2 wk after the administration of CAWS. In contrast, no significant inflammatory changes were observed in the intima or adventitia of the aorta or the coronary artery in CBA/J mice (Fig. 1, *E–H*). EVG staining revealed injuries to the elastic fibers of CBA/N mice, which developed into CAWS-vasculitis, but similar injuries were not observed in CAWS-vasculitis-resistant CBA/J mice (Fig. 2).

cDNA microarray analysis of gene expression in spleen

To determine factors that participated in the onset of CAWS-vasculitis, genome-wide patterns of gene expression in challenged mice were examined using DNA microarrays. DBA/2 was only the strain in the present experiments that died because of CAWS-vasculitis. On the other hand, CBA/J mice showed the strongest resistance to CAWS-vasculitis among the inbred strains used in these experiments. To compare the difference in gene expression in the spleen at the time of vasculitis development between DBA/2 and CBA/J mice, a comprehensive analysis of the difference among strains was performed using the oligo-DNA microarrays.

As genes showing low expression in the hybridization detection system are not reliable, spots with a sum of cyanin3 and cyanin5 fluorescence intensities exceeding 1000 and having differences of $\geq$1.5 times were selected. According to these criteria, 271 genes were up-regulated in CBA/J mice, and 148 genes were up-regulated in DBA/2 mice. Genes with unknown function in the public database were filtered out. A list of differentially expressed genes was shown in Table I. In DBA/2 mice, the expression of inflammatory genes, such as *cathepsin G*, *myeloperoxidase*, *proteinase 3*, and *neutrophil elastase*, was increased, whereas in CBA/J mice, that of *TIMP1* was increased.

As described above, DBA/2 mice are the most sensitive strain to CAWS-vasculitis, and CBA/J is the most resistant. Many inflammatory as well as anti-inflammatory genes were differentially expressed between CBA/J and DBA/2 strains, suggesting that genes responsible for inflammation may play an important role for vasculitis. In this study, a third strain, CBA/N, which exhibits Btk deficiency and it is moderately sensitive to CAWS-vasculitis, was used, as shown in Figs. 1 and 2. At present, it was decided not to carry out microarray analysis using CBA/N because of its intermediate phenotype. However, this strain is superior for quantitative experiments, as shown later (Fig. 3).

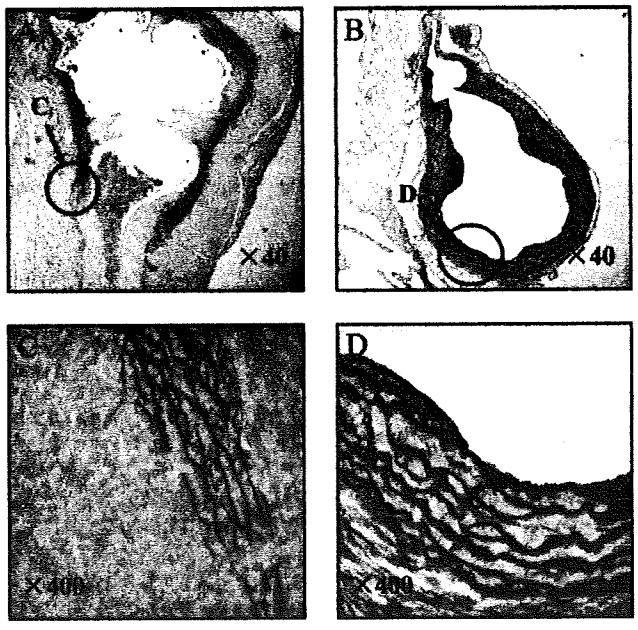

FIGURE 2. Histopathological findings of coronary arteries and aorta. CAWS (4 mg/mouse) was i.p. administered to CBA/N (*A* and *C*) and CBA/J (*B* and *D*) mice for 5 consecutive days. At 28 days after CAWS injections, mice were sacrificed and stained with EVG stain.

Blood cytokine production in the initial phase after CAWS administration

CBA/J is the only mouse strain resistant to CAWS-vasculitis among the inbred mouse strains studied so far. It was reported previously that anti-inflammatory cytokine IL-10 (23) production is increased in CBA/J mice (11). Therefore, the serum IL-10 level was measured in CBA/J and CBA/N mice after administration of CAWS (4 mg in PBS/mouse), along with the production of TIMP1, an endogenous matrix metalloprotease inhibitor, the gene expression level of which was found to be increased in the cDNA microarray analysis.

In CBA/J mice, high levels of IL-10 were produced 1 h after CAWS administration. In contrast, IL-10 production was hardly detected in CBA/N mice (Fig. 3*A*). In CBA/J mice, TIMP1 showed high levels 4 h after CAWS administration, and it continued to increase even at 10 h after CAWS administration. On the other

Table 1. *Genes differentially expressed in CBA/J and DBA/2 splenocytes at day 21*[a]

Gene Name	Log_2 Ratio	UniGene
Myeloperoxidase	3.04	Mm.4668
Neutrophilic granule protein	2.79	Mm.2827
TNF (ligand) superfamily, member 12	2.73	Mm.8983
S100 calcium-binding protein A9 (calgranulin B)	2.58	Mm.2128
Cathelicidin antimicrobial peptide	2.50	Mm.21855
Peptideglycan recognition protein	2.47	Mm.3834
Cathepsin G	2.30	Mm.4858
S100 calcium-binding protein A8 (calgranulin A)	2.27	Mm.21567
GATA-binding protein 1	2.05	Mm.1344
CD24a Ag	2.02	Mm.6417
Hemoglobin Z, β-like enbrionic chain	1.90	Mm.196718
Lipocalin 2	1.89	Mm.9537
Carbonic anhydrase 1	1.82	Mm.3471
Chemokine (C-X-C motif) ligand 7	1.62	Mm.157750
Fibronectin 1	1.51	Mm.193099
Chemokine (C-X-C motif)ligand 4	1.50	Mm.23905
Neutrophil elastase	1.39	Mm.271137
Proteinase 3	1.35	Mm.2364
Aminolevulinate, δ-,dehydratase	1.34	Mm.6988
TNF, α-induced protein 2	1.28	Mm.4348
Chemokine (C-X-C motif) receptor 4	1.18	Mm.1401
C-type lectin-like receptor 2	1.12	Mm.30700
IFN-stimulated protein	1.11	Mm.19029
Chemokine(C-X-C motif) ligand 5	0.99	Mm.4660
Chemokine (C-C motif) receptor 1-like 1	0.95	Mm.57056
IL-12R, β1	0.95	Mm.731
TGF-β1-induced transcript 4	0.94	Mm.20927
TIMP1	−5.44	Mm.8245
Insulin I	−5.20	Mm.46269
Chemokine (C-C motif) receptor 8	−4.89	Mm.8000
IL-8R, β	−4.43	Mm.234466
Carboxyl ester lipase	−4.43	Mm.4349
Carboxypeptidase B1 (tissue)	−4.30	Mm.34692
Regenerating islet-derived 2	−4.25	Mm.46360
Pancreatic lipase-related protein 2	−4.14	Mm.1230
Glycoprotein hormones, α subunit	−4.10	Mm.1361
Serine protease inhibitor, Kazal type 3	−4.04	Mm.272
Elastase 1, pancreatic	−3.97	Mm.2131
Regenerating islet-derived 1	−3.97	Mm.142731
Protease, serine, 18	−3.94	Mm.3944
Pancreatic lipase-related protein 1	−3.66	Mm.10753
Chemokine(C-X-C motif) ligand 11	−3.33	Mm.131723
Cholinergic receptor, nicotinic, β-polypeptide 1	−2.97	Mm.86425
Elastase 2	−2.92	Mm.21925
Pancreatitis-associated protein	−2.71	Mm.2553
Chymotrypsin-like	−2.70	Mm.2745
Inhibitor of κB kinase γ	−2.60	Mm.12967
Islet neogenesis-associated protein-related protein	−2.53	Mm.33691
Protease, serine, 21	−2.35	Mm.86657
TNFR superfamily, member 12a	−1.85	Mm.28518
Inter-α trypsin inhibitor, heavy chain 1	−1.75	Mm.3227
Carboxipeptidase A1	−1.64	Mm.25377
Thioredoxin 1	−1.31	Mm.260618

[a] The genes with negative ratio values are abundant in the CBA/J mice, whereas genes with positive ratio values are abundant in the DBA/2. The microarray data was deposited to Gene Expression Omnibus (accession no. GSE16529; www.ncbi.nlm.nih.gov/geo/query/acc.cgi).

hand, in CBA/N mice, TIMP1 showed high levels 4 h after CAWS administration similar to CBA/J mice, but it decreased at 10 h after CAWS administration (Fig. 3*B*).

Gene expression levels in the spleen and the aorta in the initial phase after CAWS administration

The gene expression levels of anti-inflammatory cytokines were compared in the initial phase after CAWS administration in CBA/J and CBA/N mice. CAWS (4 mg/0.2 ml PBS) was administered i.p., and the effect was examined using RT-PCR to measure IL-10 and TIMP1 gene expression levels in the spleen and the aorta 1 and 3 h after the administration (Fig. 4). β-Actin was used as the internal standard and for correcting the expression level of each sample.

IL-10 gene expression in spleen cells at 1 and 3 h after CAWS administration was higher in CBA/J mice than in CBA/N mice. In particular, high expression levels were observed 1 h after CAWS

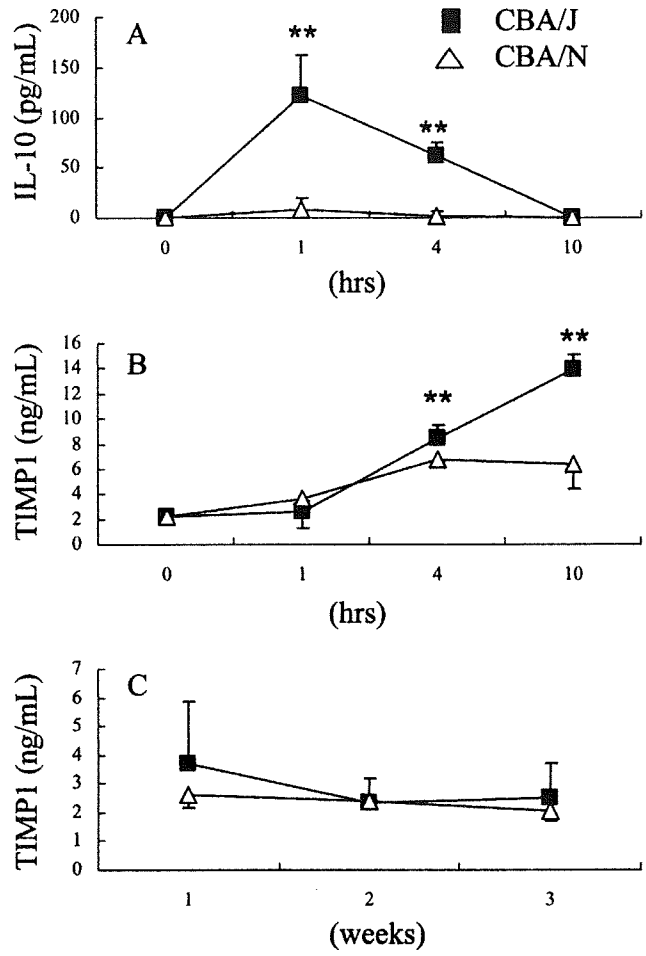

FIGURE 3. Serum IL-10 and TIMP1 leads to CAWS-injected CBA/J and CBA/N mice. Serum was collected from CBA/J and CBA/N mice i.p. injected with CAWS (4 mg/mouse) at various time points (six animals per group). IL-10 (*A*) and TIMP1 (*B*; after 0, 1, 4, 10 hours of CAWS administration, *C*; after 1, 2, 3 wk of CAWS administration) production was measured using ELISA. *, $p < 0.05$; **, $p < 0.001$ (vs 0 h).

administration. It was also observed that TIMP1 gene expression was increased in CBA/J mice after CAWS administration. However, contrary to the expectation, a particularly high expression was observed in CBA/N mice 3 h after CAWS administration (Fig. 4, *A* and *C*).

A markedly higher expression level of IL-10 gene in aorta cells of CBA/J mice was noted 1 h after CAWS administration. The IL-10 gene expression level in CBA/N mice was lower than that in CBA/J mice, but the TIMP1 gene expression level was similar in both strains before and after the administration of CAWS (Fig. 4, *B* and *D*).

Blood cytokine production in the late phase after CAWS administration

It was reported that CAWS-vasculitis begins to develop ~1 wk after CAWS administration (10). Using ELISA, serum cytokine production was measured in the late phase after CAWS administration (4 mg/0.2 ml PBS) when the vasculitis was thought to have developed (Fig. 3*C*).

IL-10 production was not observed in either CBA/J or CBA/N mice in the late phase after CAWS administration (data not shown). After 1 wk of CAWS administration, TIMP1 production in CBA/J mice tended to be higher but not to a significant degree.

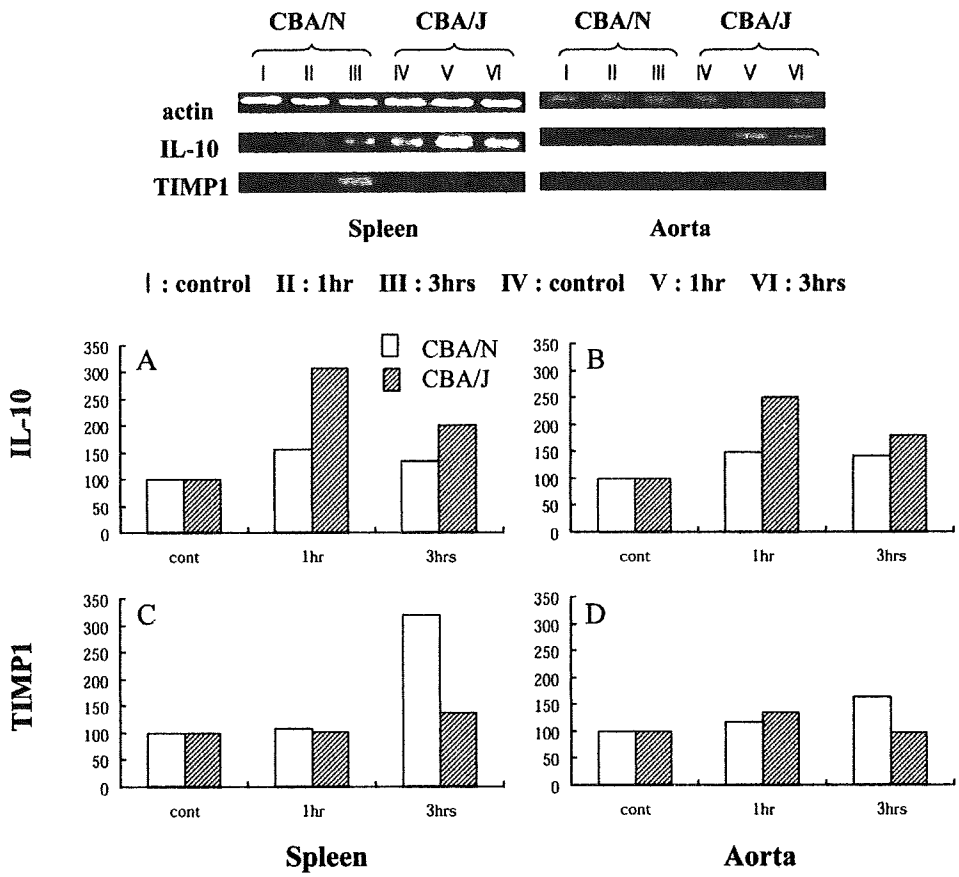

FIGURE 4. Semiquantitative analysis of IL-10 and TIMP1 mRNA expression ratios relative to actin in the spleen and aorta. Total RNA was isolated from the spleen and the aorta of CBA/J and CBA/N mice i.p. injected with CAWS (0 or 4 mg/mouse) at various time points. After the reverse transcriptase reaction was performed, each gene expression level was measured by semiquantitative PCR. Actin mRNA expression was also measured as an internal control and used for the normalized of target genes expression levels. *A*, IL-10 mRNA expression level in the spleen; *B*, IL-10 mRNA expression level in the aorta; *C*, TIMP1 mRNA expression level in the spleen; and *D*, TIMP1 mRNA expression level in the aorta.

TIMP1 production in CBA/J mice was not different from that in CBA/N mice after 2 or 3 wk of CAWS administration.

Gene expression in the spleen and the aorta in late phase after CAWS administration

IL-10 and TIMP1 gene expression levels were compared in the spleen and the aorta of CBA/J and CBA/N mice during the vasculitis-forming phase after CAWS administration. CAWS (4 mg/0.2 ml PBS) was administered i.p. for 5 consecutive days, and IL-10 and TIMP1 gene expression levels were examined by RT-PCR in the spleen and the aorta 2 and 4 wk after the last administration.

High IL-10 gene expression levels were observed in both the spleen and the aorta of CBA/J mice 2 wk after CAWS administration (Fig. 5). On the other hand, no IL-10 gene expression was observed in CBA/N mice. High TIMP1 gene expression was noted in the aorta of CBA/J mice 2 and 4 wk after CAWS administration. In addition, in the late phase after CAWS administration, the gene expression level in the spleen and the aorta showed a similar pattern.

Cytokine production in spleen cells of CBA/J and CBA/N mice after stimulation with pathogen-associated molecular patterns (PAMP)

Previous studies have indicated that when spleen cells of DBA/2 and CBA/J mice in which vasculitis had been induced by CAWS were cultured with CAWS the production of non-anti-inflammatory cytokines but not inflammatory cytokines was observed in DBA/2 mice, whereas the production of non-inflammatory cytokines but not anti-inflammatory cytokine IL-10 was observed in CBA/J mice (11). Therefore, the production of IL-10 and inflammatory cytokines IL-6 and IFN-γ was studied in CBA/J and CBA/N mice. The following PAMP were used: LPS, a Gram-negative bacterial cell wall component recognized by TLR4; PAM3, which is recognized by TLR2; and CpG, a synthetic oligodeoxynucleotide recognized by TLR9.

Upon stimulation with these PAMP recognized by respective TLR, the production of a large amount of IL-10 was observed in the spleen cells of CBA/J mice, which show resistance to CAWS-vasculitis. The production of IL-6 and IFN-γ was hardly observed in the spleen cells of CBA/J mice. On the other hand, in the spleen cells of CBA/N mice, which are sensitive to CAWS-vasculitis, the production of IL-6 and IFN-γ but not IL-10 was observed (Fig. 6).

Acute lethal activity in CAWS-administered mice

Other than its vasculitis-inducing activity, CAWS is known for its acute lethal activity after i.v. administration (12, 13). As a positive control, a closed colony of ICR mice was used, in which ~100% acute lethal activity is observed. A 200-μg acute lethal dose of CAWS was administered to the closed-colony ICR mice, in addition to 400 μg of CAWS, which is double that amount, through the caudal vein of the mice.

The acute lethal activity of CAWS was clearly observed in vasculitis-resistant CBA/J mice. CBA/J mice showed reduced movement ~5 min after CAWS administration and shock status ~15 min after administration. Almost all the mice died within 25 min after administration. In contrast, no acute lethal activity was observed in vasculitis-sensitive CBA/N mice, and acute lethal activity was also not observed in DBA/2 mice that develop severe vasculitis (Table II).

Discussion

Kawasaki disease induces the development of systemic vasculitis. In particular, the vasculitis that develops in the coronary artery

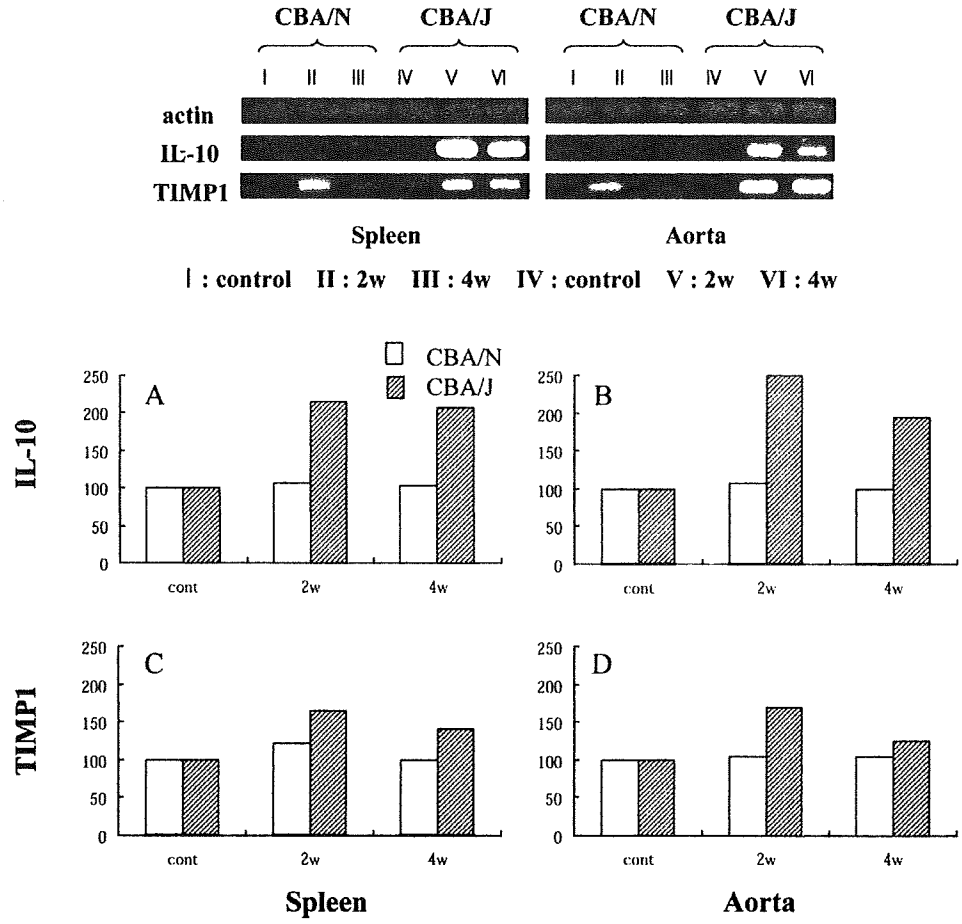

FIGURE 5. Semiquantitative analysis of IL-10 and TIMP1 mRNA expression ratios relative to actin in the spleen and the aorta. Total RNA was isolated from the spleen and the aorta of CBA/J and CBA/N mice i.p. injected with CAWS (0 or 4 mg/mouse) at various time points. After the reverse transcriptase reaction was performed, each gene expression level was measured by semiquantitative PCR. Actin mRNA expression level was also measured as an internal control and used for the normalized of target genes expression levels. *A*, IL-10 mRNA expression level in the spleen; *B*, IL-10 mRNA expression level in the aorta; *C*, TIMP1 mRNA expression level in the spleen; and *D*, TIMP1 mRNA expression level in the aorta.

sometimes becomes lethal, and thus, elucidation of the mechanisms underlying its pathogenesis and therapy is clinically important. According to Murata and colleagues (5–7), when CAWS is i.p. administered daily, vasculitis in the coronary artery, similar to that in Kawasaki disease, can be induced at a high rate. Although the vasculitis-inducing activity of CAWS has been studied in various inbred mouse strains, it was revealed for the first time that CAWS-vasculitis can be induced in Btk-deficient CBA/N mice (Figs. 1 and 2). Analysis of serial sections of the aorta stained with H&E suggested that the vasculitis in CBA/N mice was mild compared with that in DBA/2 mice, because aortic stenosis was mild and no reduction in survival rate was observe after CAWS administration (10, 14). Previous studies have shown that elastic fiber injury occurs in the aorta close to the beginning of the coronary artery in mice that develop CAWS-vasculitis (10). A similar phenomenon was observed in CBA/N mice as well. Because such a phenomenon was not observed in CAWS-vasculitis-resistant CBA/J mice, a rupture of the elastic fibers in CBA/N mice was thought to be attributable to CAWS-vasculitis. The aorta is an elastic-type artery, and this elasticity is due to the formation of a substantial elastic layer in the tunica media. The upper part of the aorta where CAWS-vasculitis occurs is particularly rich in elastic fibers. Therefore, the present observation that injury occurs in the aortic elastic fibers in CBA/N mice as a result of CAWS-vasculitis is an important finding for further analysis of CAWS-vasculitis in the future.

CBA/J mice showed resistance to CAWS-vasculitis. To the best of our knowledge, no inbred mouse strain, except for CBA/J, is resistant to CAWS-vasculitis. Therefore, further analysis of resistance to CAWS-vasculitis in CBA/J mice is considered to be important not only for the elucidation of the pathogenic mechanism of CAWS-vasculitis but also for the development of a therapeutic model. On the other hand, DBA/2 mice develop severe vasculitis following CAWS administration, and this vasculitis is fatal. No other strains of mice, except for DBA/2, showed fatal CAWS-vasculitis. To determine the factors that participated in the onset of CAWS-vasculitis, mRNA expression in the splenocytes from DBA/2 and CBA/J mice was examined using a microarray technique. High expression levels of mRNA such as myeloperoxidase, cathepsin G, neutrophil elastase, and proteinase 3 were recognized in DBA/2 mice. These proteins are well-known markers of neutrophils and correlate with inflammation.

TIMP1 was suggested to be one of the most important factors in the inhibition of CAWS-vasculitis in the results of the microarray analysis (Table I). TIMP1 is known to be a MMP-specific endogenous inhibitor. Contrary to expectation, temporarily high levels of TIMP1 were observed in CBA/J mice (Fig. 3). It was reported that there was no correlation between blood TIMP and MMP production levels and disease severity in multiple patients with Kawasaki disease, and an imbalance of these levels contributed to the development of vasculitis (24, 25). It was also suggested that the imbalance of TIMP and MMP is a factor contributing to the development of vasculitis. MMP was reported to be involved in vasculitis remodeling and the formation of vasculitis in Kawasaki disease (26). Therefore, further studies may be necessary to examine not only TIMP levels per se but also its production level relative to MMP.

The gene expression levels of IL-10 and TIMP1 in spleen and aortic root were examined at early and late stages of CAWS-vasculitis (Figs. 4 and 5). In the late stage (2–4 wk after CAWS

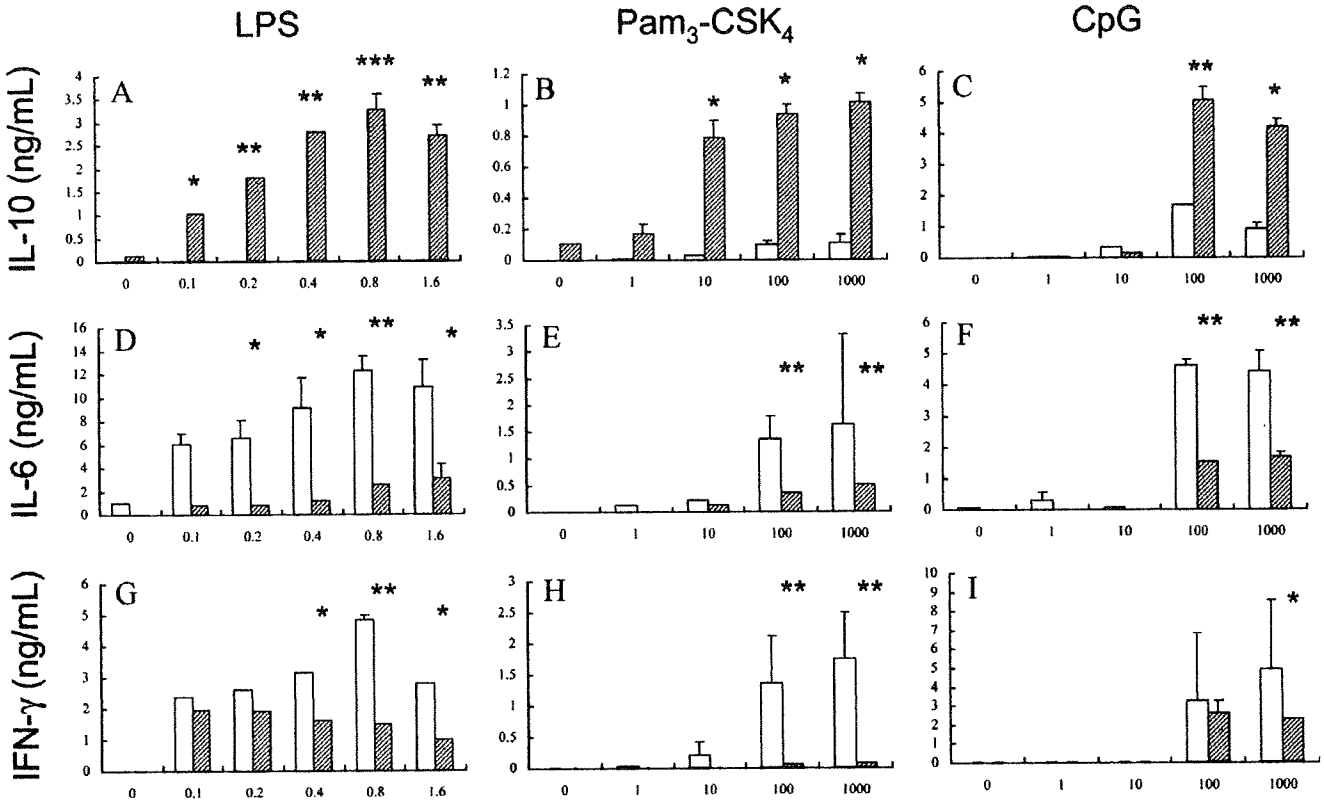

FIGURE 6. Cytokine production in culture supernatants of splenocytes from CBA/J and CBA/N mice stimulated with LPS, PAM_3-CSK_4, and CpG-oligodeoxynucleotide. Splenocytes were collected from CBA/J and CBA/N mice (four animals per group). Prepared splenocytes were cultured with LPS (0, 0.1, 0.2, 0.4, 0.8, or 1.6 μg/ml, *A*, *D*, *G*), PAM_3-CSK_4 (0, 1, 10, 100, or 1000 ng/ml, *B*, *E*, *H*), or CpG-ODN (0, 1, 10, 100, or 1000 nM, *C*, *F*, *I*) for 48 h at an initial density of 5×10^6 cells/ml. The culture supernatants were collected and measured for IL-10 (*A–C*), IL-6 (*D–F*), and IFN-γ (*G–I*) levels using ELISA. □, CBA/N; ▨, CBA/J. *, $p < 0.05$; **, $p < 0.001$ (vs blank).

administration), CAWS-vasculitis had developed, and the infiltration of leukocytes in CBA/N mice was significant. In contrast, leukocyte infiltration into the aortic root was scarce in CBA/J mice (Figs. 1 and 2). It was of interest that both IL-10 and TIMP1 were highly expressed in the aortic root of CBA/J mice. IL-10 acts as anti-inflammatory, and TIMP1 protects tissues from proteases; thus, the expression of both genes concomitantly protects the tissue from inflammation. In the case of CBA/N mice, TIMP1 was expressed weakly, but no IL-10 expression could be detected. The anti-inflammatory system of the aortic root could be weak. Of interest, gene expression in the aortic root and spleen are similar for both genes, suggesting that inflammatory and/or anti-inflammatory states may not be local but systemic. In the early stage of CAWS-vasculitis, when leukocyte infiltration is scarcely induced in both strains of mice, both IL-10 and TIMP1 expression levels were also high in CBA/J mice. From both the results of early and late stages, it was suggested that cells expressing IL-10 and TIMP1 may not be infiltrating inflammatory cells but resident cells of the aortic tissue, such as endothelial cells, fibroblasts, and smooth muscle cells, as well as resident macrophages. However, precise characterization of the cells expressing anti-inflammatory cytokines and molecules was not performed in this study.

Table II. *Acute lethal toxicity of CAWS i.v. administrated mice*[a]

	CBA/J	CBA/N	DBA/2	ICR
200 μg/mouse	4/5	0/5	0/5	5/5
400 μg/mouse	5/5	0/5	0/5	5/5

[a] The acute lethal toxicity of CAWS was monitored after i.v. administration to ICR mice and observing the mice that died within 1 h after administration.

Stimulation of spleen cells of both CBA/J and CBA/N mice with various PAMP revealed high IL-10 production in the spleen cells of CBA/J mice (Fig. 6). It is known that PAMP are mainly recognized by TLR on the cell surface (27). On the other hand, IL-10 was barely produced in the spleen cells of CBA/N mice, whereas the production of inflammatory cytokines IL-6 and IFN-γ was observed. Such cytokine responses are thought to be a factor contributing to the development of CAWS-vasculitis in CBA/N mice. As described earlier, CBA/N mice have a genetic background lacking Btk compared with wild-type CBA/J mice. Therefore, it was strongly suggested that Btk is involved in the difference in IL-10 production between the two mouse strains.

As a result of studies on acute lethal activity after CAWS administration in various inbred mouse strains, in which vasculitis-inducing activity is obvious, this study observed acute lethal activity in vasculitis-resistant CBA/J mice. In contrast, vasculitis-sensitive CBA/N and DBA/2 mice did not show acute lethal activity (Table II). Although the mechanism underlying the development of acute lethal activity has not been completely elucidated, the fact that CAWS is a mannoprotein-β-glucan complex suggests that the complement lectin pathway is involved (28). It was also speculated that in accordance with the activation of the complement lectin pathway by CAWS, anaphylatoxin production and subsequent production of platelet-activating factor (PAF) are activated. PAF is suggested to play an important role in the shock observed when yeast mannan is administered (29). It was reported that PAF receptor induces the production of IL-10 (30–34). However, it remains unknown whether Btk, which is the genetic

difference between CBA/J and CBA/N mice, affects these pathways or not.

From these results, CBA/J mice are thought to be resistant to vasculitis because the inhibitory pathway, including IL-10, is easily induced not only by CAWS but also by various ligands.

Acknowledgments

We thank Hiroki Sankawa for excellent technical assistance.

Disclosures

The authors have no financial conflict of interest.

References

1. Kawasaki, T., and F. Kousaki. 1967. Febrile oculo-oro-cutaneo-acrodesquamatous syndrome with or without acute nonsuppurative cervical lymphadenitis in infancy and childhood: clinical observations of 50 cases (in Japanese). *Jpn. J. Allergy* 16: 178–222.
2. Newburger, J. W., M. Takahashi, M. A. Gerber, M. H. Gewitz, L. Y. Tani, J. C. Burns, S. T. Shulman, A. F. Bolger, P. Ferrieri, R. S. Baltimore, et al. 2004. Diagnosis, treatment, and long-term management of Kawasaki disease: a statement for health professionals from the Committee on Rheumatic Fever, Endocarditis and Kawasaki Disease, Council on Cardiovascular Disease in the Young, American Heart Association. *Circulation* 110: 2747–2771.
3. Newburger, J. W., M. Takahashi, A. S. Beiser, J. C. Burns, J. Bastian, K. J. Chung, S. D. Colan, C. E. Duffy, D. R. Fulton, and M. P. Glode. 1991. A single intravenous infusion of gammaglobulin as compared with four infusions in the treatment of acute Kawasaki syndrome. *N. Engl. J. Med.* 324: 1633–1639.
4. Furusho, K., T. Kamiya, H. Nakano, N. Kiyosawa, K. Shinomiya, T. Hayashidera, T. Tamura, O. Hirose, Y. Manabe, and T. Yokoyama. 1984. High-dose intravenous gammaglobulin for Kawasaki disease. *Lancet* 2: 1055–1058.
5. Murata, H., H. Iijima, S. Naoe, T. Atobe, T. Uchiyama, and S. Arakawa. 1987. The pathogenesis of experimental arteritis induced by *Candida* alkali extract in mice. *Jpn. J. Exp. Med.* 57: 305–313.
6. Murata, H., and S. Naoe. 1987. Experimental *Candida*-induced arteritis in mice—relation to arteritis in Kawasaki disease. *Prog. Clin. Biol. Res.* 250: 523.
7. Takahashi, K., T. Oharaseki, M. Wakayama, Y. Yokouchi, S. Naoe, and H. Murata. 2004. Histopathological features of murine systemic vasculitis caused by *Candida albicans* extract—an animal model of Kawasaki Disease. *Inflamm. Res.* 53: 72–77.
8. Ohno, N. 2008. A murine model of vasculitis induced by fungal polysaccharide. *Cardiovasc. Hematol. Agents Med. Chem.* 6: 44–52.
9. Ohno, N. 2006. Models of Kawasaki disease. *Drug Discov. Today Dis. Models* 3: 83–89.
10. Hirata, N., K. Ishibashi, S. Ohta, S. Hata, H. Shinohara, M. Kitamura, N. Miura, and N. Ohno. 2006. Histopathological examination and analysis of mortality in DBA/2 mouse vasculitis induced with CAWS, a water-soluble extracellular polysaccharide fraction obtained from *Candida albicans*. *Yakugaku Zasshi* 126: 643–650.
11. Nagi-Miura, N., Y. Shingo, Y. Adachi, A. Ishida-Okawara, T. Oharaseki, K. Takahashi, S. Naoe, K. Suzuki, and N. Ohno. 2004. Induction of coronary arteritis with administration of CAWS (*Candida albicans* water-soluble fraction) depending on mouse strains. *Immunopharmacol. Immunotoxicol.* 26: 527–543.
12. Kurihara, K., N. N. Miura, M. Uchiyama, N. Ohno, Y. Adachi, M. Aizawa, H. Tamura, S. Tanaka, and T. Yadomae. 2000. Measurement of blood clearance time by Limulus G test of *Candida*-water soluble polysaccharide fraction, CAWS, in mice. *FEMS Immunol. Med. Microbiol.* 29: 69–76.
13. Kurihara, K., Y. Shingo, N. N. Miura, S. Horie, Y. Usui, Y. Adachi, T. Yadomae, and N. Ohno. 2003. Effect of CAWS, a mannoprotein-β-glucan complex of *Candida albicans*, on leukocyte, endothelial cell, and platelet functions in vitro. *Biol. Pharm. Bull.* 26: 233–240.
14. Nagi-Miura, N., T. Harada, H. Shinohara, K. Kurihara, Y. Adachi, A. Ishida-Okawara, T. Oharaseki, K. Takahashi, S. Naoe, K. Suzuki, and N. Ohno. 2006. Lethal and severe coronary arteritis in DBA/2 mice induced by fungal pathogen, CAWS. *Candida albicans* water-soluble fraction. *Atherosclerosis* 186: 310–320.
15. Ishida-Okawara, A., N. Nagi-Miura, T. Oharaseki, K. Takahashi, A. Okumura, H. Tachikawa, S. Kashiwamura, H. Okamura, N. Ohno, H. Okada, et al. 2007. Neutrophil activation and arteritis induced by *C. albicans* water-soluble mannoprotein-β-glucan complex (CAWS). *Exp. Mol. Pathol.* 82: 220–226.
16. Kanegane, H., K. Nomura, T. Futatani, and T. Miyawaki. 2002. Intravenous immunoglobulin replacement therapy in X-linked agammaglobulinemia (in Japanese; includes abstract). *Jpn. J. Clin. Immun.* 25: 337–343.
17. Berning, A. K., E. M. Eicher, W. E. Paul, and I. Scher. 1980. Mapping of the X-linked immune deficiency mutation (*xid*) of CBA/N mice. *J. Immunol.* 124: 1875–1877.
18. Cancro, M. P., A. P. Sah, S. L. Levy, D. M. Allman, M. R. Schmidt, and R. T. Woodland. 2001. *xid* mice reveal the interplay of homeostasis and Bruton's tyrosine kinase-mediated selection at multiple stages of B cell development. *Int. Immunol.* 13: 1501–1514.
19. Middendorp, S., G. M. Dingjan, A. Maas, K. Dahlenborg, and R. W. Hendriks. 2003. Function of Bruton's tyrosine kinase during B cell development is partially independent of its catalytic activity. *J. Immunol.* 171: 5988–5996.
20. Satterthwaite, A. B., and O. N. Witte. 2000. The role of Bruton's tyrosine kinase in B cell development and function: a genetic perspective. *Immunol. Rev.* 175: 120–127.
21. Mukhopadhyay, S., M. Mohanty, A. Mangla, A. George, V. Bal, S. Rath, and B. Ravindran. 1999. Bruton's tyrosine kinase deficiency in macrophages inhibits nitric oxide generation leading to enhancement of IL-12 induction. *J. Immunol.* 163: 1786–1792.
22. Koike, M., Y. Kikuchi, A. Tominaga, S. Takaki, K. Akagi, J. Miyazaki, K. Yamamura, and K. Takatsu. 1995. Defective IL-5-receptor-mediated signaling in B cells of X-linked immunodeficient mice. *Int. Immunol.* 7: 21–30.
23. Moore, K. W., R. de Waal Malefyt, R. L. Coffman, and A. O'Garra. 2001. Interleukin-10 and the interleukin-10 receptor. *Annu. Rev. Immunol.* 19: 683–765.
24. Senzaki, H., S. Masutani, J. Kobayashi, T. Kobayashi, H. Nakano, H. Nagasaka, N. Sasaki, H. Asano, S. Kyo, and Y. Yokote. 2004. Circulating matrix metalloproteinases and their inhibitors in patients with Kawasaki disease. *Circulation* 104: 860–863.
25. Chua, P. K., M. E. Melish, Q. Yu, R. Yanagihara, K. S. Yamamoto, and V. R. Nerurkar. 2003. Elevated levels of matrix metalloproteinase 9 and tissue inhibitor of metalloproteinase 1 during the acute phase of Kawasaki disease. *Clin. Diagn. Lab. Immunol.* 10: 308–314.
26. Gavin, P. J., S. E. Crawford, S. T. Shulman, F. L. Garcia, and A. H. Rowley. 2003. Systemic arterial expression of matrix metalloproteinases 2 and 9 in acute Kawasaki disease. *Arterioscler. Thromb. Vasc. Biol.* 23: 576–581.
27. Jefferies, C. A., and L. A. O'Neill. 2004. Bruton's tyrosine kinase (Btk)—the critical tyrosine kinase in LPS signalling? *Immunol. Lett.* 92: 15–22.
28. Shinohara, H., N. Nagi-Miura, K. Ishibashi, Y. Adachi, A. Ishida-Okawara, T. Oharaseki, K. Takahashi, S. Naoe, K. Suzuki, and N. Ohno. 2006. β-Mannosyl linkages negatively regulate anaphylaxis and vasculitis in mice, induced by CAWS, fungal PAMPs composed of mannoprotein-β-glucan complex secreted by *Candida albicans*. *Biol. Pharm. Bull.* 29: 1854–1861.
29. Mikami, T., K. Fukushi, M. Ishitani, K. Ishitani, S. Suzuki, and M. Suzuki. 1991. Induction of platelet-activating factor in mice by intravenous administration of a neutral fraction of bakers' yeast mannan. *Lipids* 26: 1404–1407.
30. Zhang, Q., N. Mousdicas, Q. Yi, M. Al-Hassani, S. D. Billings, S. M. Perkins, K. M. Howard, S. Ishii, T. Shimizu, and J. B. Travers. 2005. Staphylococcal lipoteichoic acid inhibits delayed-type hypersensitivity reactions via the platelet-activating factor receptor. *J. Clin. Invest.* 115: 2855–2861.
31. Pei, Y., L. A. Barber, R. C. Murphy, C. A. Johnson, S. W. Kelley, L. C. Dy, R. H. Fertel, T. M. Nguyen, D. A. Williams, and J. B. Travers. 1998. Activation of the epidermal platelet-activating factor receptor results in cytokine and cyclooxygenase-2 biosynthesis. *J. Immunol.* 161: 1954–1961.
32. Dy, L. C., Y. Pei, and J. B. Travers. 1999. Augmentation of ultraviolet B radiation-induced tumor necrosis factor production by the epidermal platelet-activating factor receptor. *J. Biol. Chem.* 274: 26917–26921.
33. Southall, M. D., J. S. Isenberg, H. Nakshatri, Q. Yi, Y. Pei, D. F. Spandau, and J. B. Travers. 2001. The platelet-activating factor receptor protects epidermal cells from tumor necrosis factor (TNF) α and TNF-related apoptosis-inducing ligand-induced apoptosis through an NF-κB-dependent process. *J. Biol. Chem.* 276: 45548–45554.
34. Walterscheid, J. P., S. E. Ullrich, and D. X. Nghiem. 2002. Platelet-activating factor, a molecular sensor for cellular damage, activates systemic immune suppression. *J. Exp. Med.* 195: 171–179.